Electronic Supplementary Material (ESI) for Journal of Materials Chemistry C.

Supporting Information for:

Design of functionalized luminescent MOF sensor for precise monitoring of tuberculosis drug and neonicotinoid pesticide from human body-fluids and food samples to protect health and environment

*Abhijeet Rana,[a] Nazir Ud Din Mir,[a] Arpa Banik,[b] Ananya Hazra,[a] and Shyam Biswas[a]**

[a] Department of Chemistry, Indian Institute of Technology Guwahati, Guwahati, 781039, Assam, India.

[b] Department of Chemistry, Indian Institute of Science Educational and Research, Berhampur, 760003, Odisha, India

*Corresponding author. Tel: 91-3612583309, Fax: 91-3612582349. E-mail address: sbiswas@iitg.ac.in

Materials and Characterization Methods:

The linker 2-(((2-hydroxy naphthalene-1-yl)methyl)amino)terephthalic acid (H_2L) was synthesized according to the previously reported procedure.[1] All other required chemicals were purchased from commercial sources and used without further purification. The Attenuated Total Reflectance Infrared (ATR-IR) spectra were recorded using PerkinElmer UATR Two at the ambient condition in the region 400-4000 cm^{-1}. The notations used for the characterization of the bands are broad (br), strong (s), very strong (vs), medium (m), weak (w) and shoulder (sh). Thermogravimetric (TA) experiments were conducted with a heating rate of 4 °C min^{-1} oxygen atmosphere in PerkinElmer, TGA 4000, thermogravimetric analyser thermogravimetric analyser. Rigaku Smartlab X-ray diffractometer (model TTRAX III) with Cu-Kα radiation (λ = 1.54056 Å), 40 kV of operating voltage and 125 mA of operating current was used to collect all PXRD data. The specific surface area for N_2 sorption was calculated on a Quantachrome Autosorb iQMP gas sorption analyzer at -196 °C. FE-SEM and EDX images were collected with a Zeiss (Sigma 300) scanning electron microscope. The DICVOL program incorporated within STOE's WinXPow software package was used to determine the lattice parameters. Dimond 5.0 was used for drawing the crystal structure of **1′**. Fluorescence sensing studies were performed with a HORIBA JOBIN YVON Fluoromax-4 spectrofluorometer. Fluorescence lifetimes were measured using Picosecond Time-resolved and Steady State Luminescence Spectrometer on an Edinburg Instruments Lifespec II & FSP 920 instrument. Solution state UV-Vis spectra were measured using PerkinElmer Lamda 365 + instrument. Automated ultra-high vacuum X-ray photoelectron spectroscopy of **1′** was carried out using PHI 5000 versa probe III spectrophotometer.

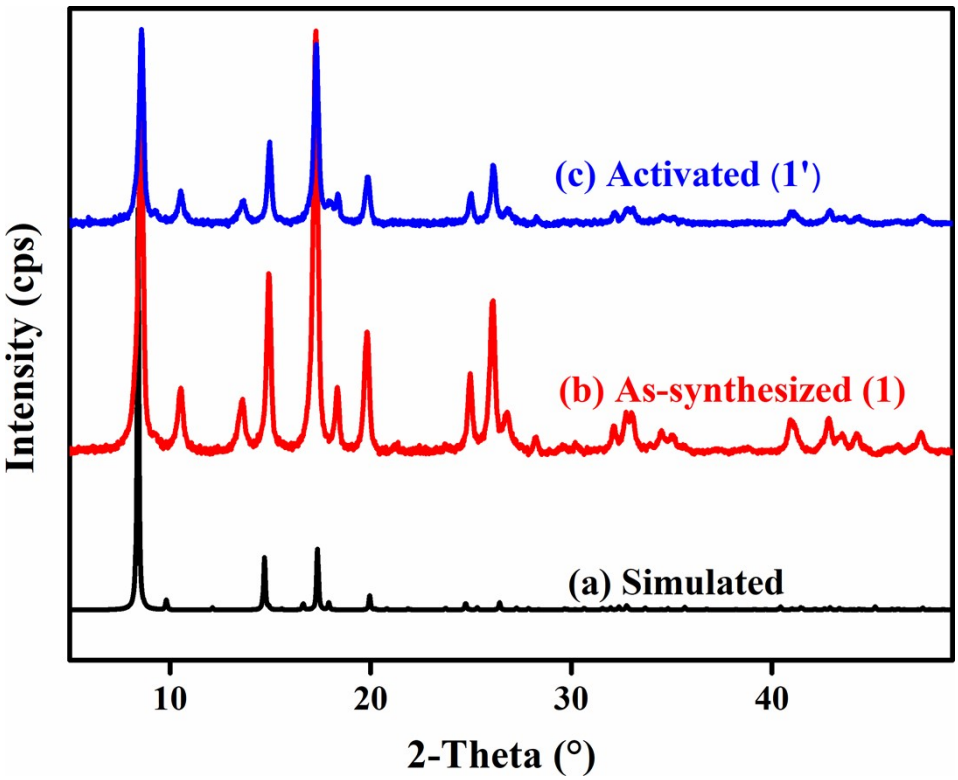

Figure S1. The PXRD patterns of simulated MIL-53 (black), as-synthesized **1** (red) and activated **1'** (blue).

Table S1. Unit cell parameters of simulated MIL-53(Al) and **1**.

Compound Name	**[Al(OH)(L)]·0.5H_2O (1)** (this work)	MIL-53(Al) (reported)
Crystal System	Orthorhombic P	Orthorhombic P
a ≠ b ≠ c (Å)	16.654 ≠ 12.890 ≠ 6.610 (9)	16.675 ≠ 12.813 ≠ 6.608 (2)
α = β = γ (°)	90	90
V ($Å^3$)	1419.1 (17)	1411.8 (2)
Radiation	Cu Kα1	Cu Kα1

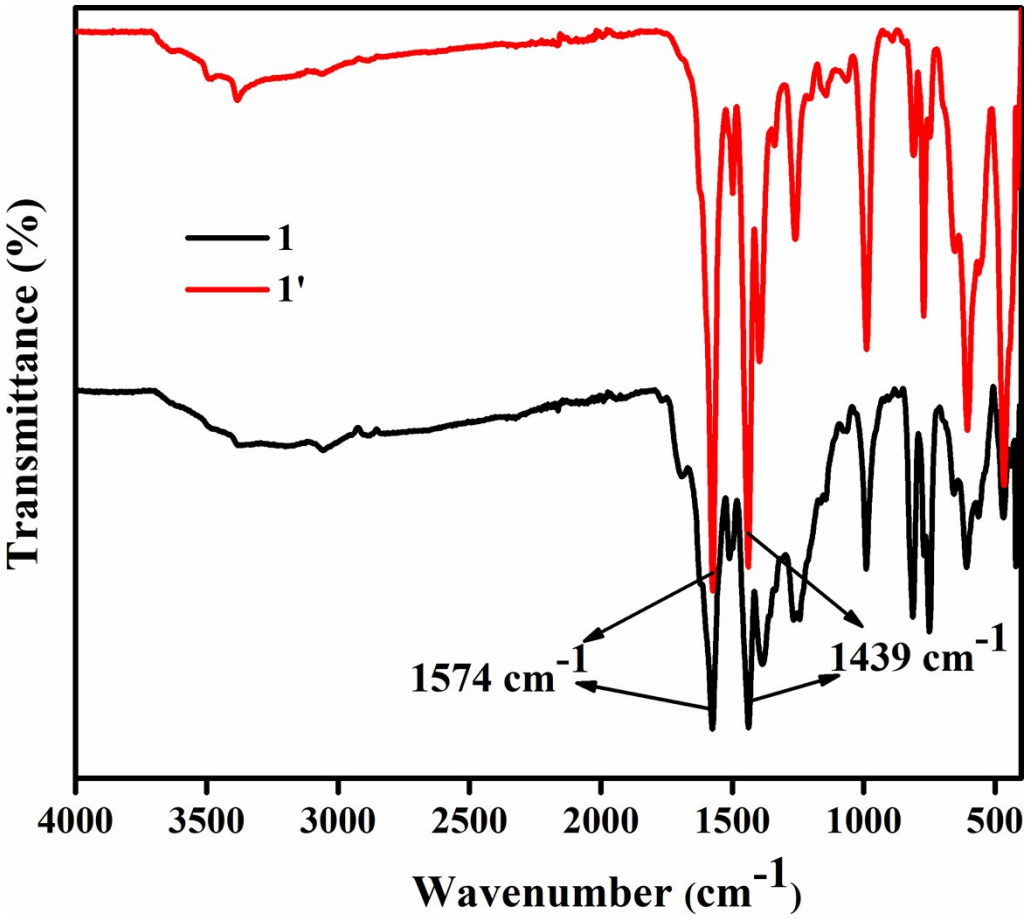

Figure S2. ATR-IR spectrum of **1** (red) and **1'**(black).

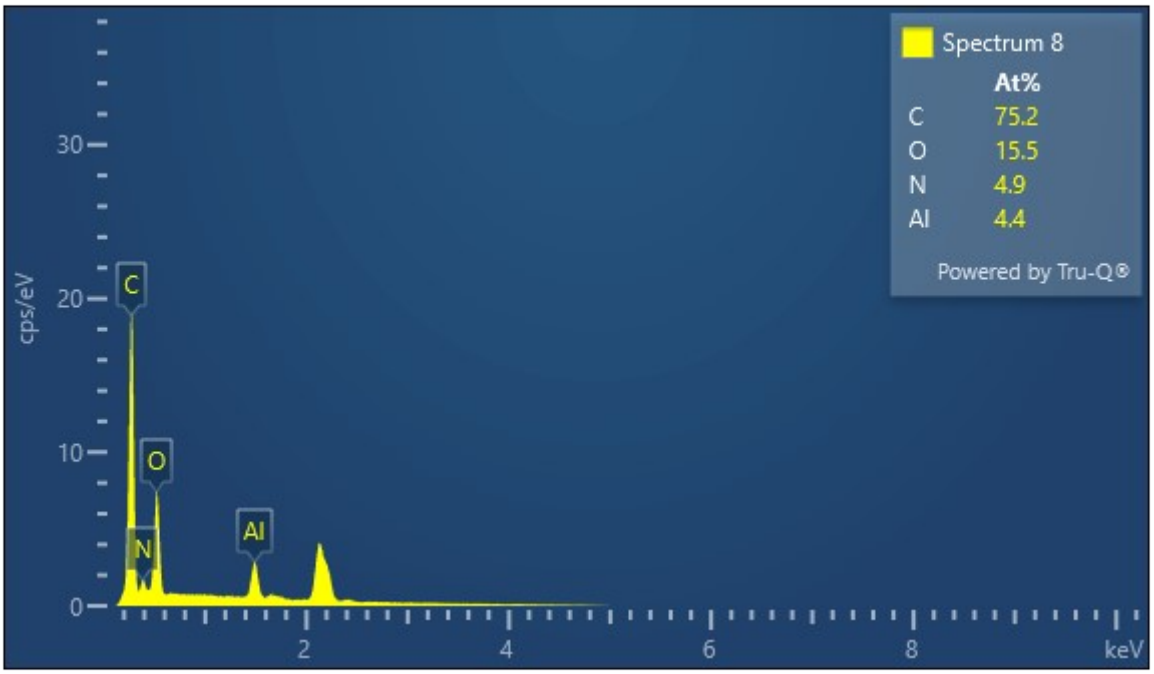

Figure S3. EDX spectrum of **1'**.

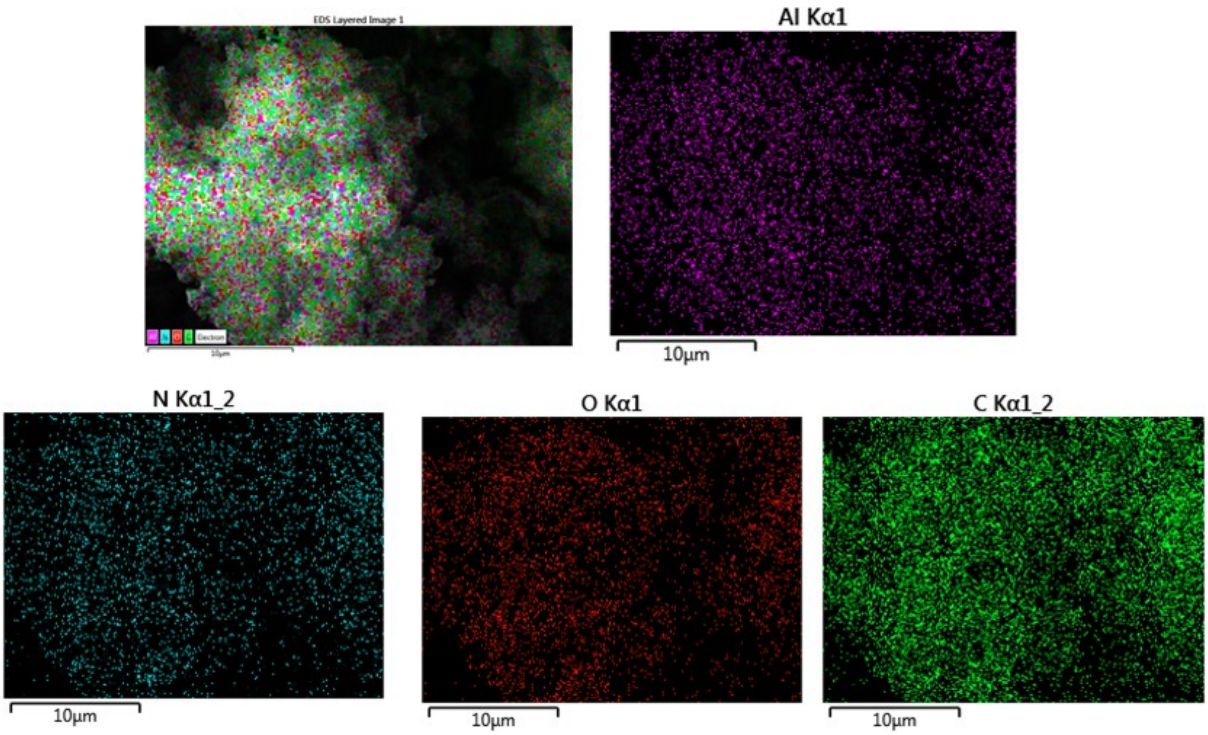

Figure S4. EDX elemental mapping of **1'**.

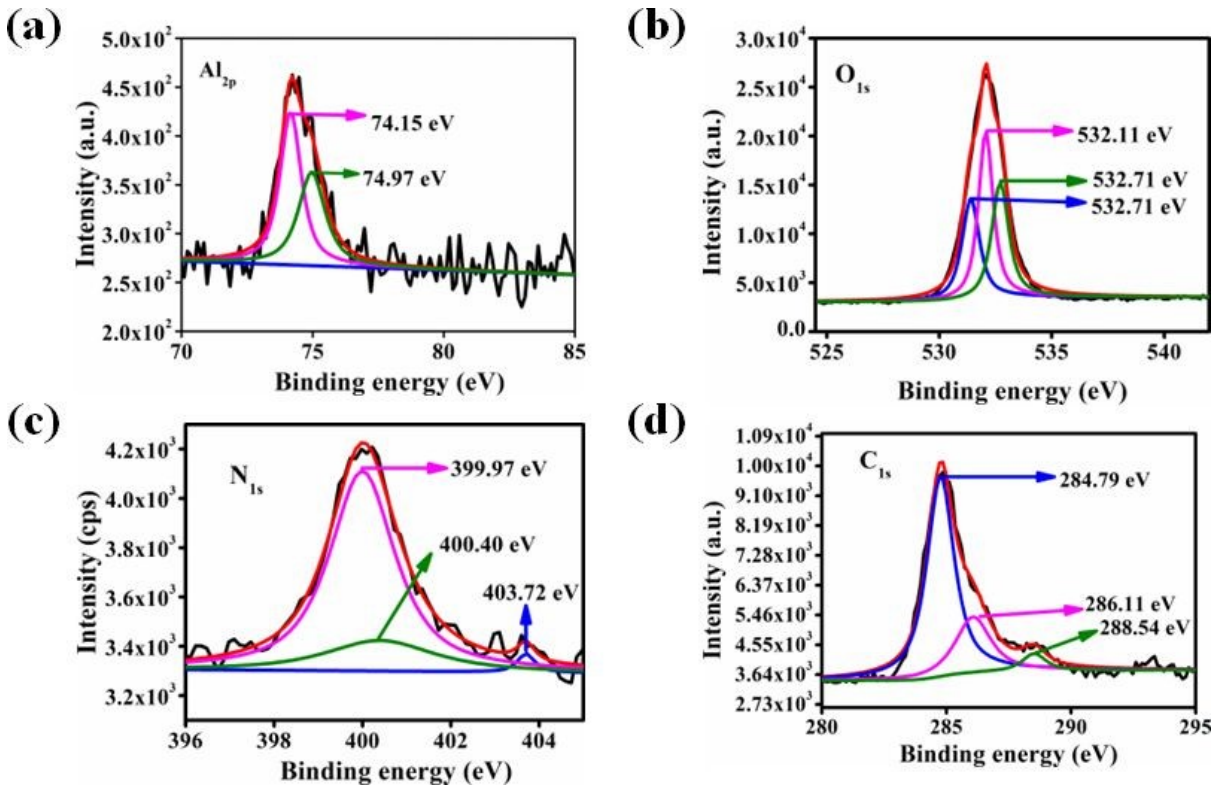

Figure S5. XPS spectra of the elements of **1'**.

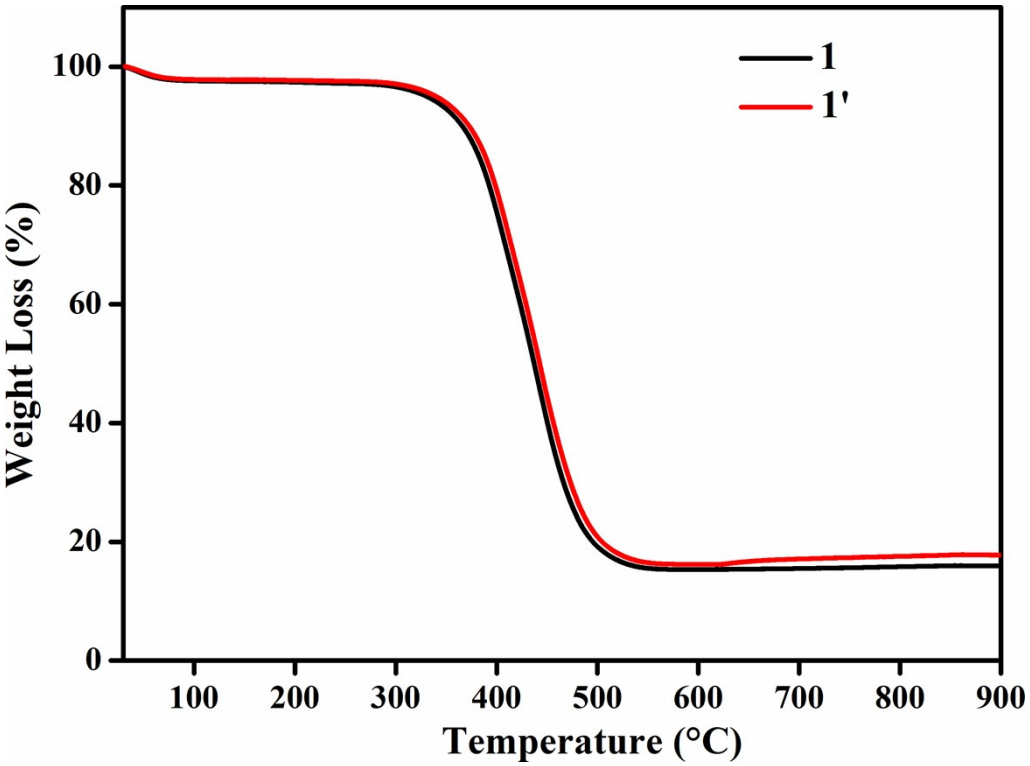

Figure S6. Thermogravimetric analysis of **1** (red) and **1'** (black).

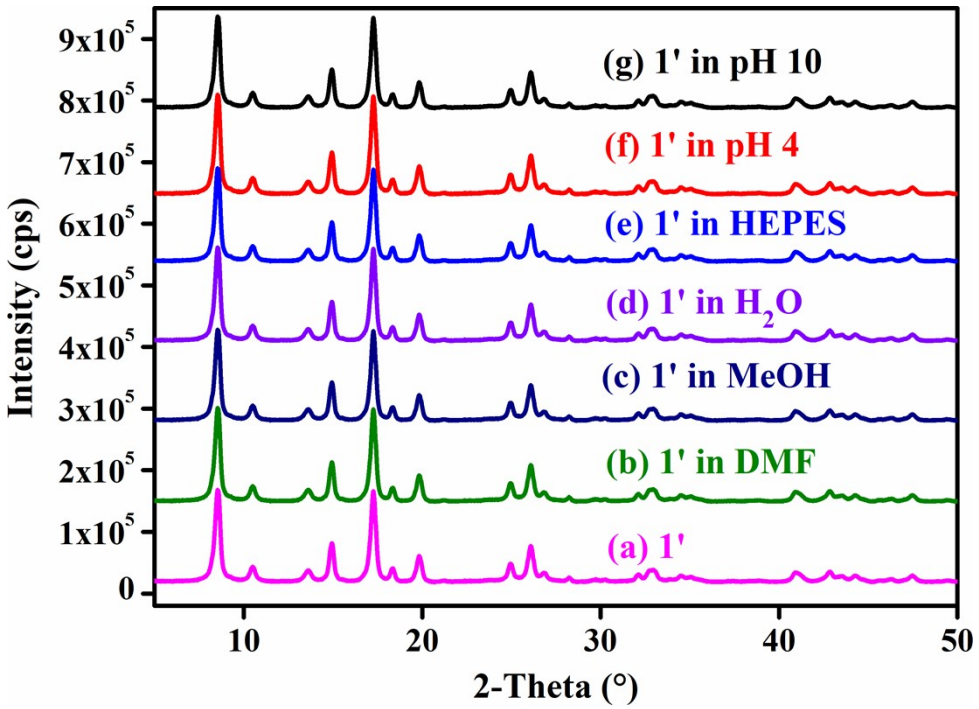

Figure S7. PXRD pattern of **1'** after stirring in different organic solvents and pH media for 24 h.

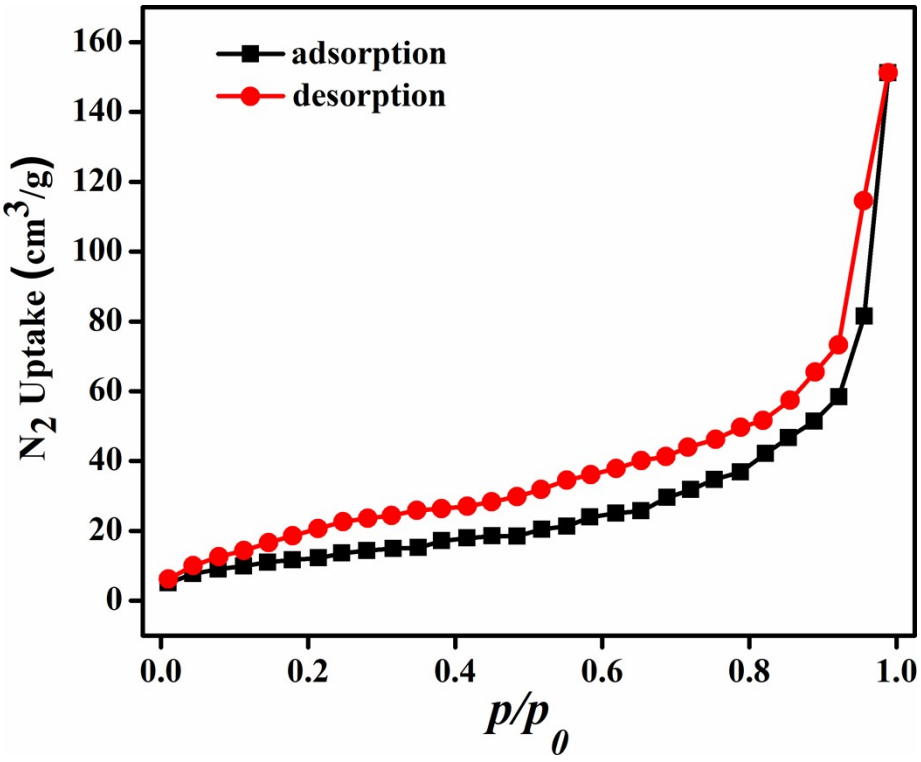

Figure S8. N_2 sorption isotherm of **1'**.

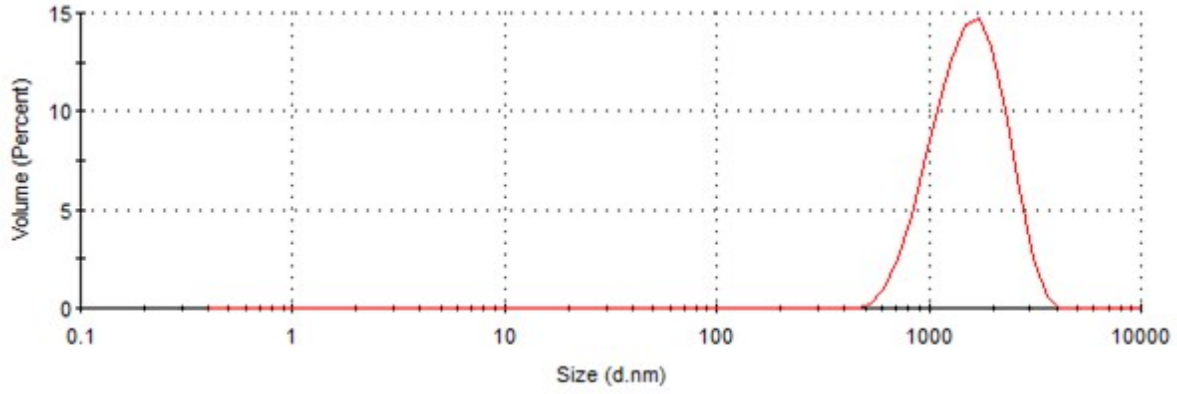

Figure S9. Particle size distribution curve of **1'** in aqueous medium from DLS measurement.

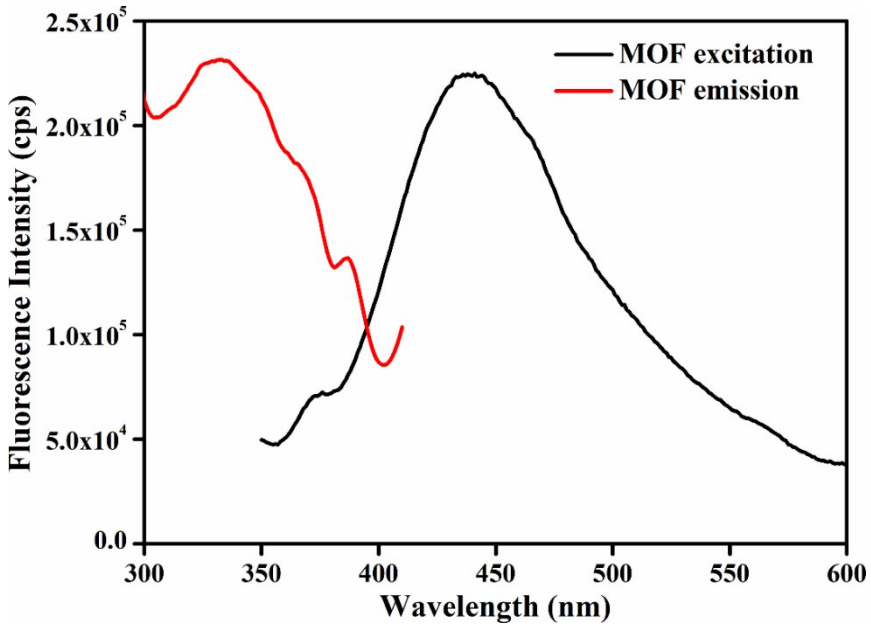

Figure S10. Excitation and emission spectra of **1'** in water.

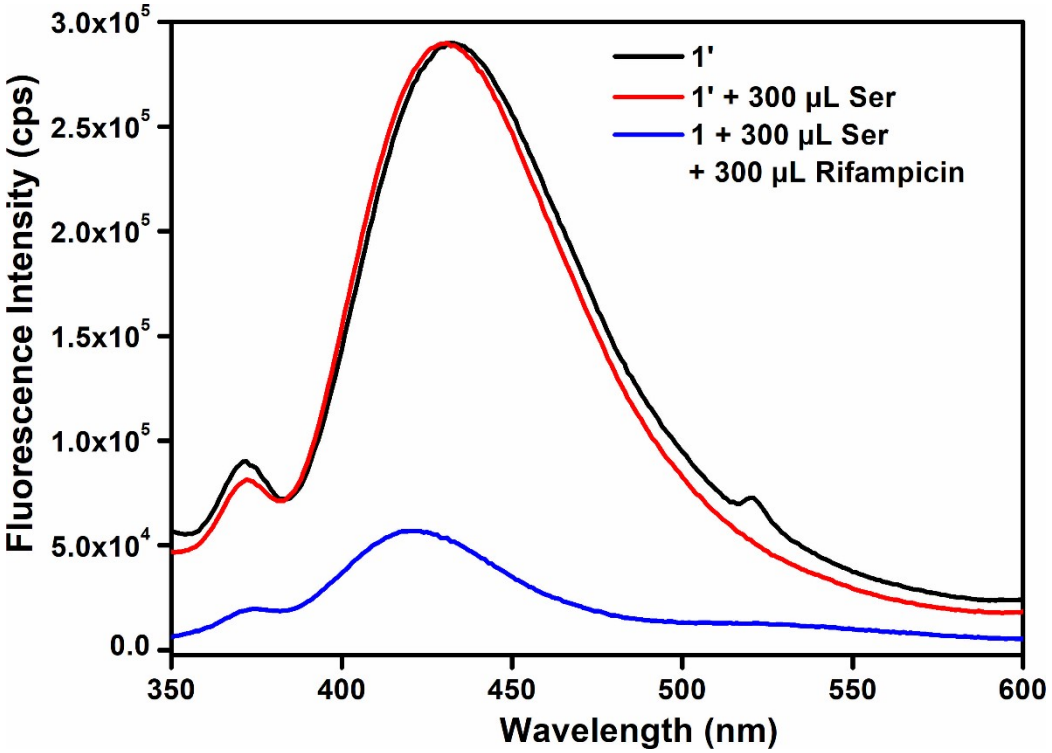

Figure S11. Fluorescence emission intensity of **1'** (black), **1'** in the presence of 300 µL of 1 mM aqueous serine solution (red) and **1'** in the presence of both 300 µL of 1 mM aqueous serine and rifampicin solution (blue).

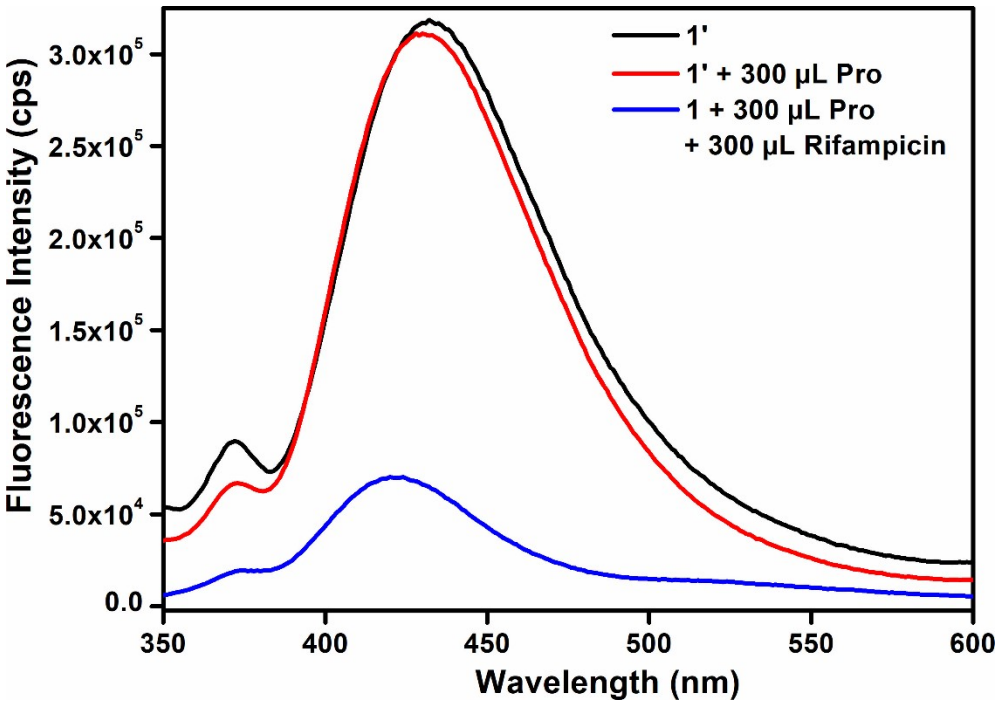

Figure S12. Fluorescence emission intensity of **1'** (black), **1'** in the presence of 300 µL of 1 mM aqueous proline solution (red) and **1'** in the presence of both 300 µL of 1 mM aqueous proline and rifampicin solution (blue).

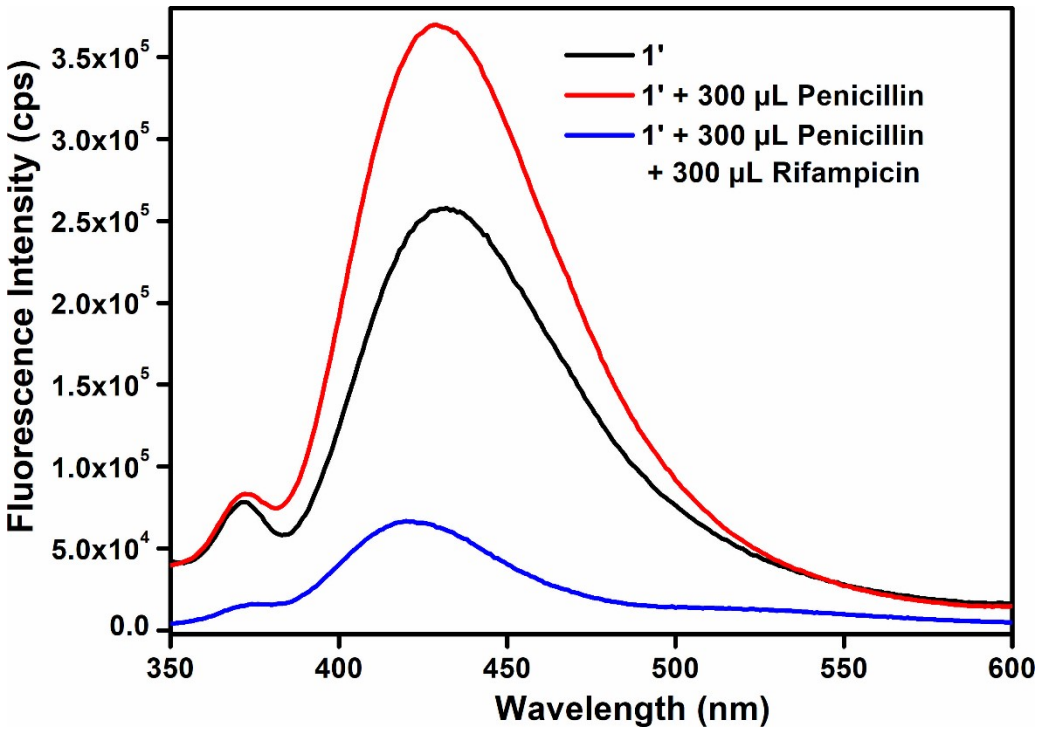

Figure S13. Fluorescence emission intensity of **1'** (black), **1'** in the presence of 300 µL of 1 mM aqueous penicillin solution (red) and **1'** in the presence of both 300 µL of 1 mM aqueous penicillin and rifampicin solution (blue).

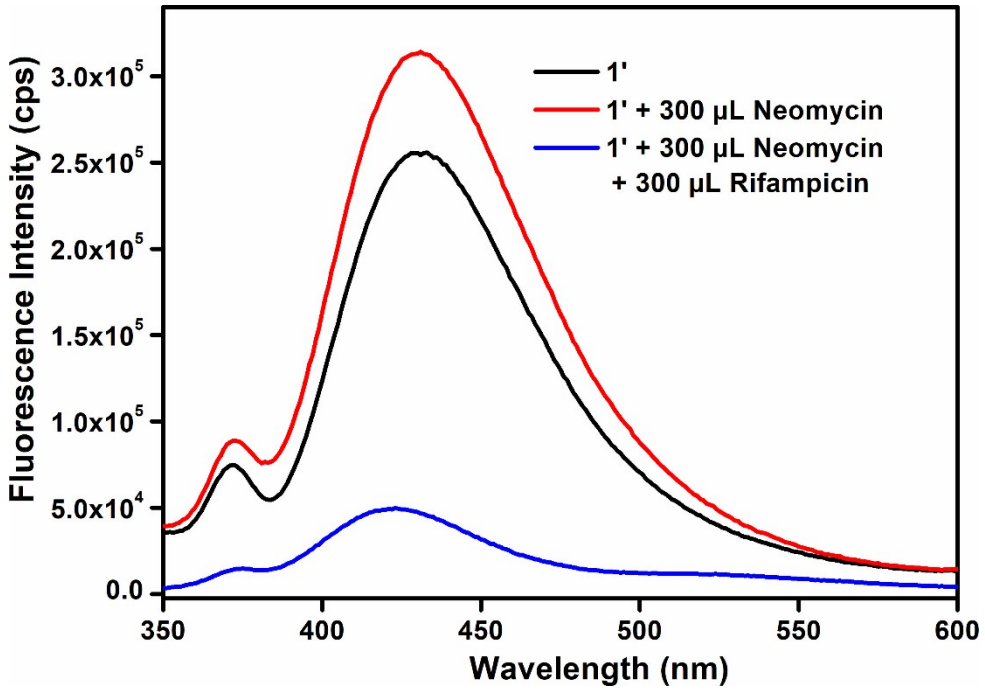

Figure S14. Fluorescence emission intensity of **1'** (black), **1'** in the presence of 300 µL of 1 mM aqueous neomycin solution (red) and **1'** in the presence of both 300 µL of 1 mM aqueous neomycin and rifampicin solution (blue).

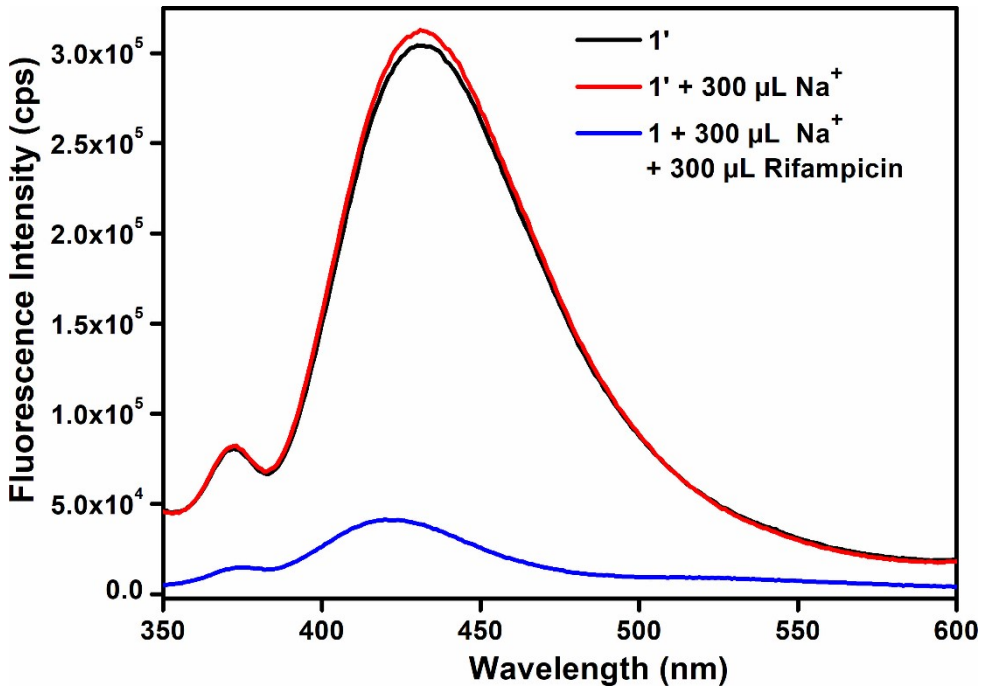

Figure S15. Fluorescence emission intensity of **1'** (black), **1'** in the presence of 300 µL of 1 mM aqueous Na^+ solution (red) and **1'** in the presence of both 300 µL of 1 mM aqueous Na^+ and rifampicin solution (blue).

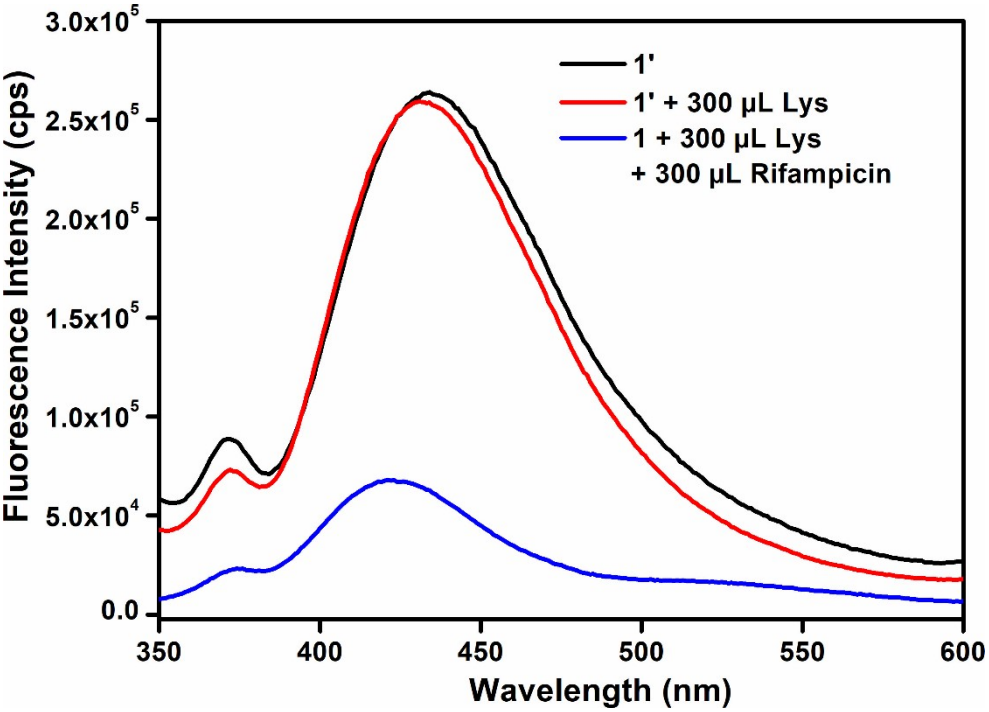

Figure S16. Fluorescence emission intensity of **1'** (black), **1'** in the presence of 300 µL of 1 mM aqueous lysine solution (red) and **1'** in the presence of both 300 µL of 1 mM aqueous lysine and rifampicin solution (blue).

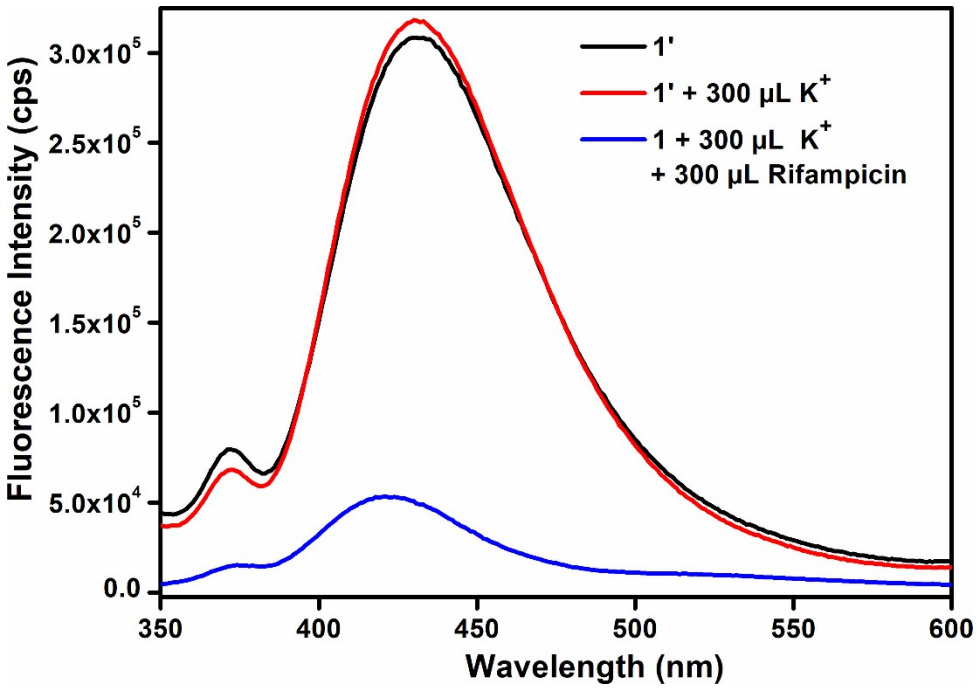

Figure S17. Fluorescence emission intensity of **1'** (black), **1'** in the presence of 300 µL of 1 mM aqueous K^+ solution (red) and **1'** in the presence of both 300 µL of 1 mM aqueous K^+ and rifampicin solution (blue).

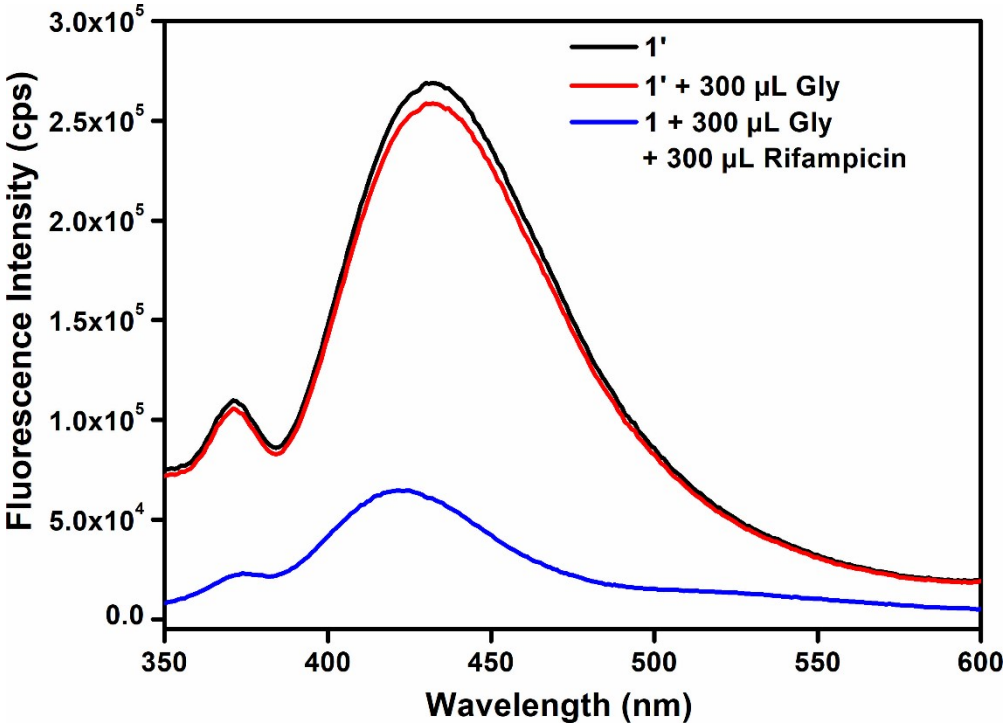

Figure S18. Fluorescence emission intensity of **1'** (black), **1'** in the presence of 300 µL of 1 mM aqueous glycine solution (red) and **1'** in the presence of both 300 µL of 1 mM aqueous glycine and rifampicin solution (blue).

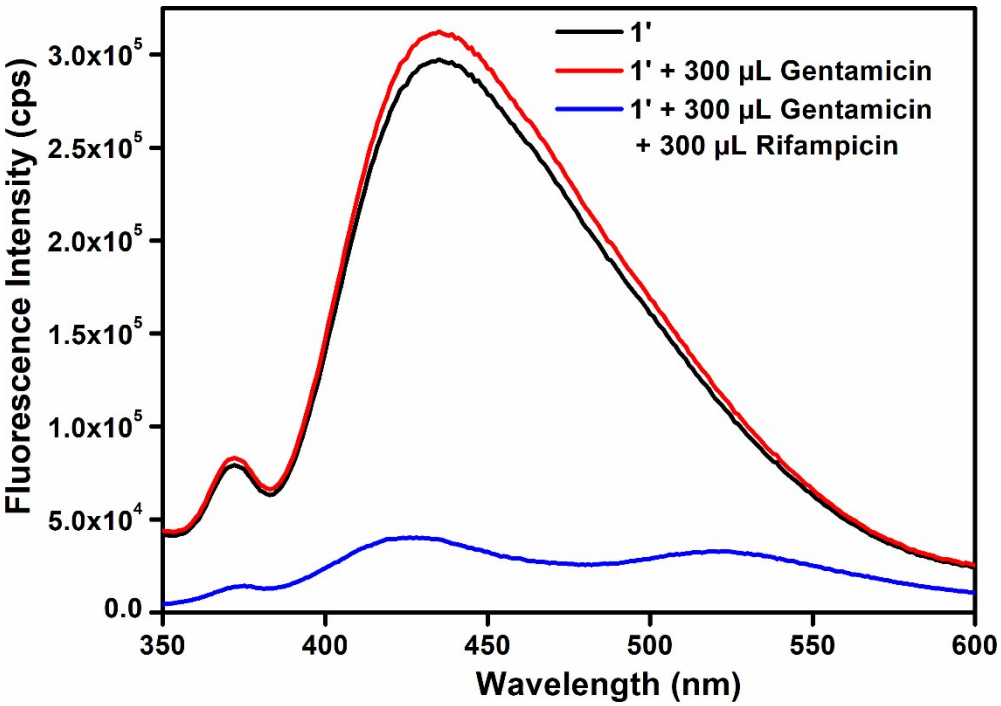

Figure S19. Fluorescence emission intensity of **1'** (black), **1'** in the presence of 300 µL of 1 mM aqueous gentamicin solution (red) and **1'** in the presence of both 300 µL of 1 mM aqueous gentamicin and rifampicin solution (blue).

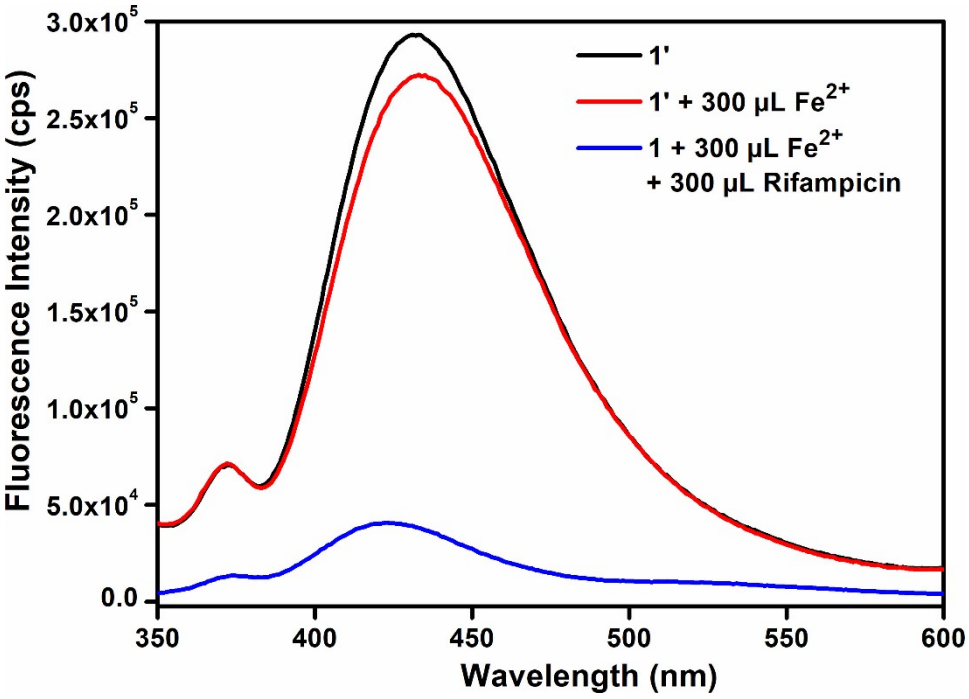

Figure S20. Fluorescence emission intensity of **1'** (black), **1'** in the presence of 300 µL of 1 mM aqueous Fe^{2+} solution (red) and **1'** in the presence of both 300 µL of 1 mM aqueous Fe^{2+} and rifampicin solution (blue).

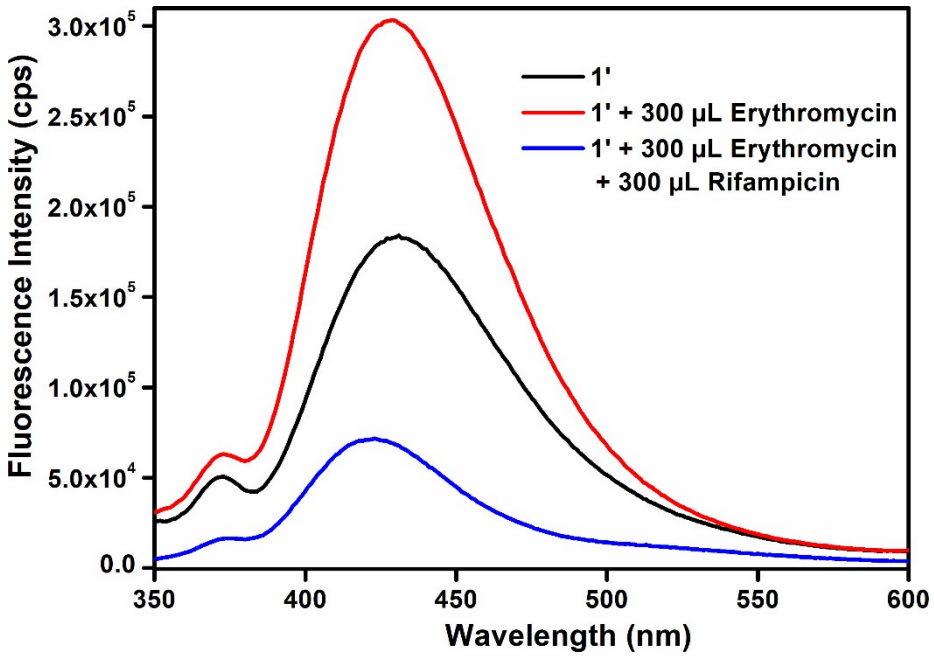

Figure S21. Fluorescence emission intensity of **1'** (black), **1'** in the presence of 300 µL of 1 mM aqueous erythromycin solution (red) and **1'** in the presence of both 300 µL of 1 mM aqueous erythromycin and rifampicin solution (blue).

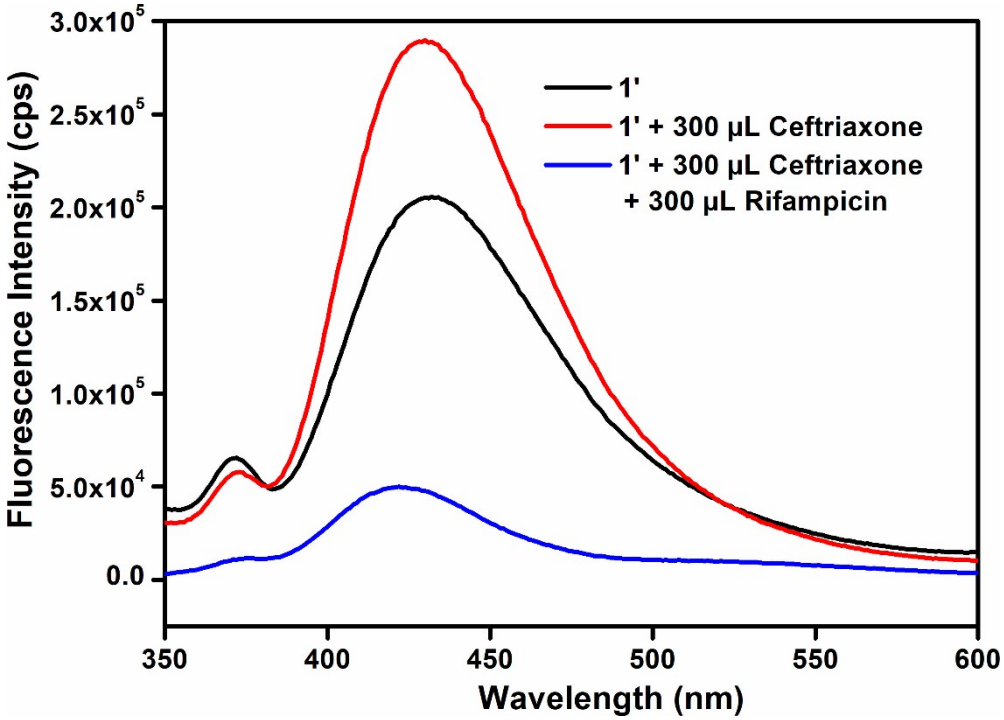

Figure S22. Fluorescence emission intensity of **1'** (black), **1'** in the presence of 300 µL of 1 mM aqueous ceftriaxone solution (red) and **1'** in the presence of both 300 µL of 1 mM aqueous ceftriaxone and rifampicin solution (blue).

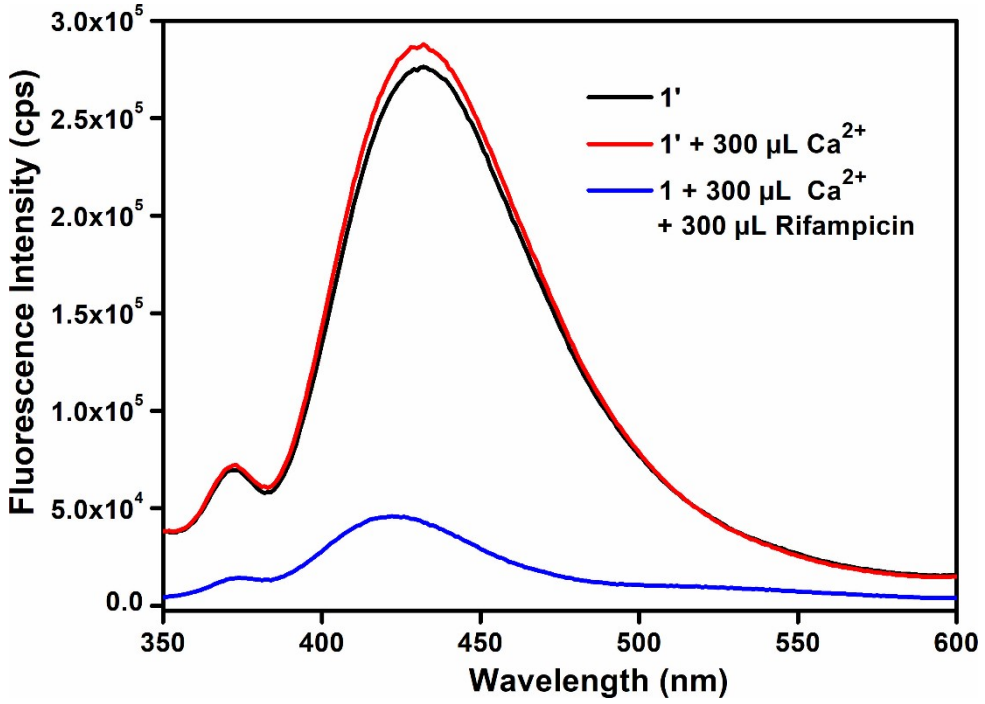

Figure S23. Fluorescence emission intensity of **1'** (black), **1'** in the presence of 300 µL of 1 mM aqueous Ca^{2+} solution (red) and **1'** in the presence of both 300 µL of 1 mM aqueous Ca^{2+} and rifampicin solution (blue).

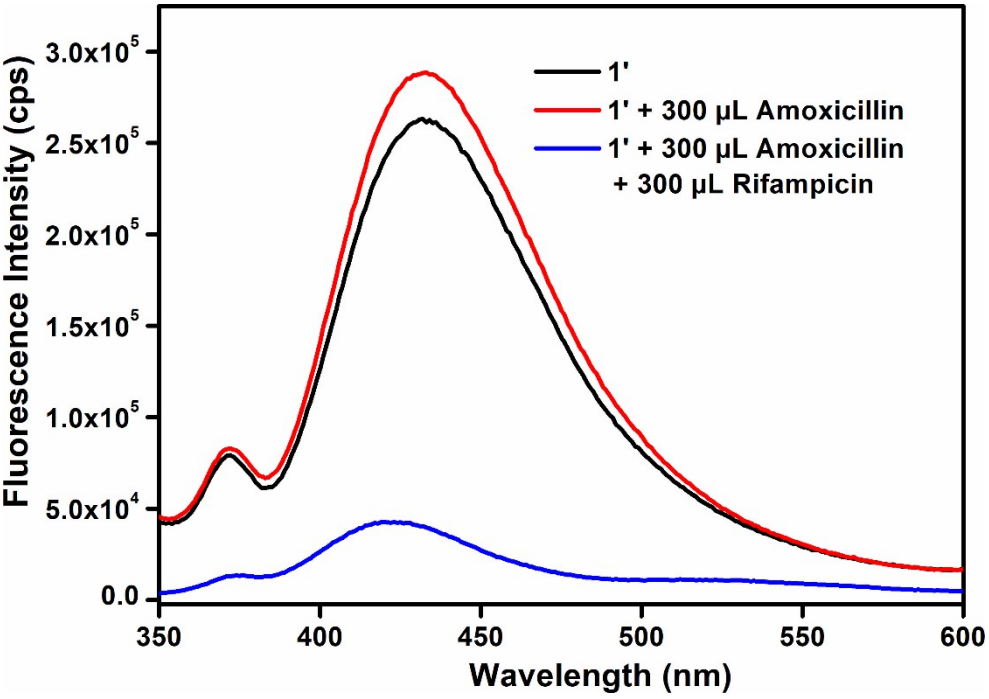

Figure S24. Fluorescence emission intensity of **1'** (black), **1'** in the presence of 300 µL of 1 mM aqueous amoxicillin solution (red) and **1'** in the presence of both 300 µL of 1 mM aqueous amoxicillin and rifampicin solution (blue).

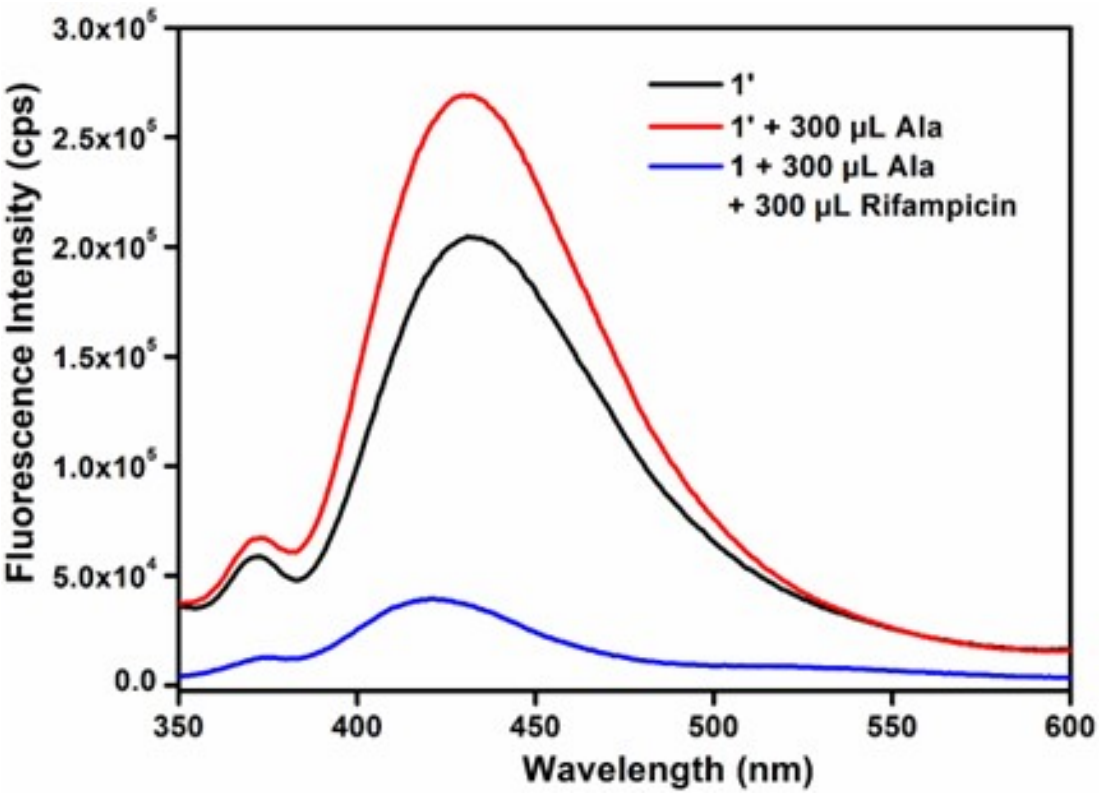

Figure S25. Fluorescence emission intensity of **1'** (black), **1'** in the presence of 300 µL of 1 mM aqueous alanine solution (red) and **1'** in the presence of both 300 µL of 1 mM aqueous alanine and rifampicin solution (blue).

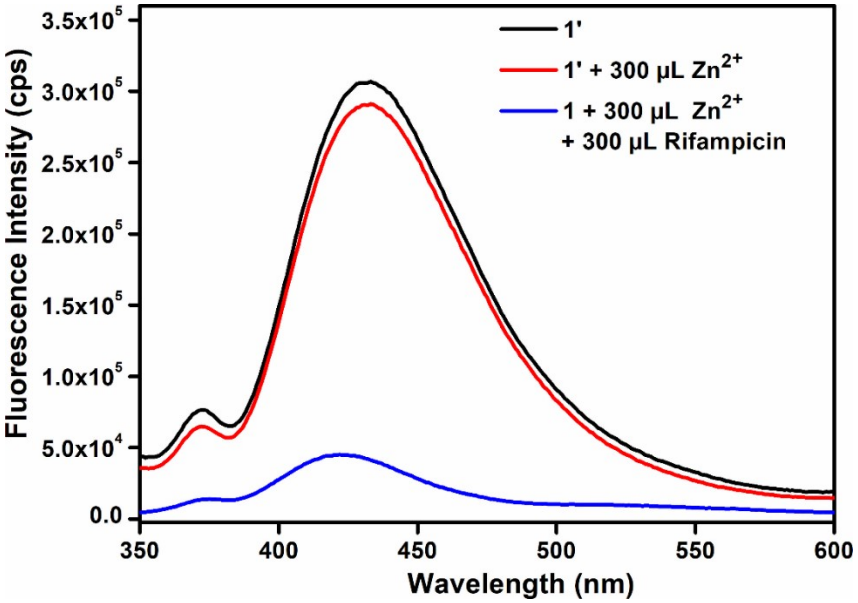

Figure S26. Fluorescence emission intensity of **1'** (black), **1'** in the presence of 300 µL of 1 mM aqueous Zn^{2+} solution (red) and **1'** in the presence of both 300 µL of 1 mM aqueous Zn^{2+} and rifampicin solution (blue).

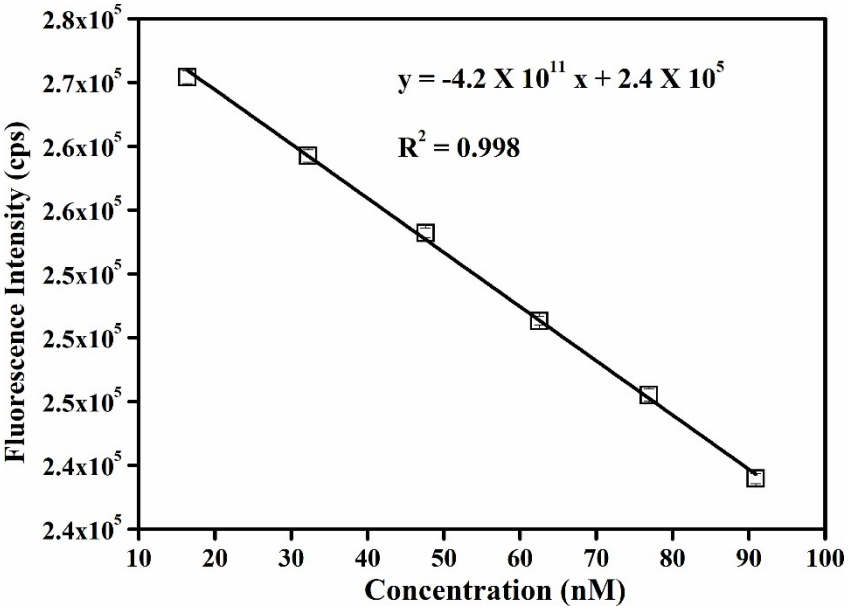

Figure S27. Plot of concentration of rifampicin versus fluorescence intensity of **1′**.

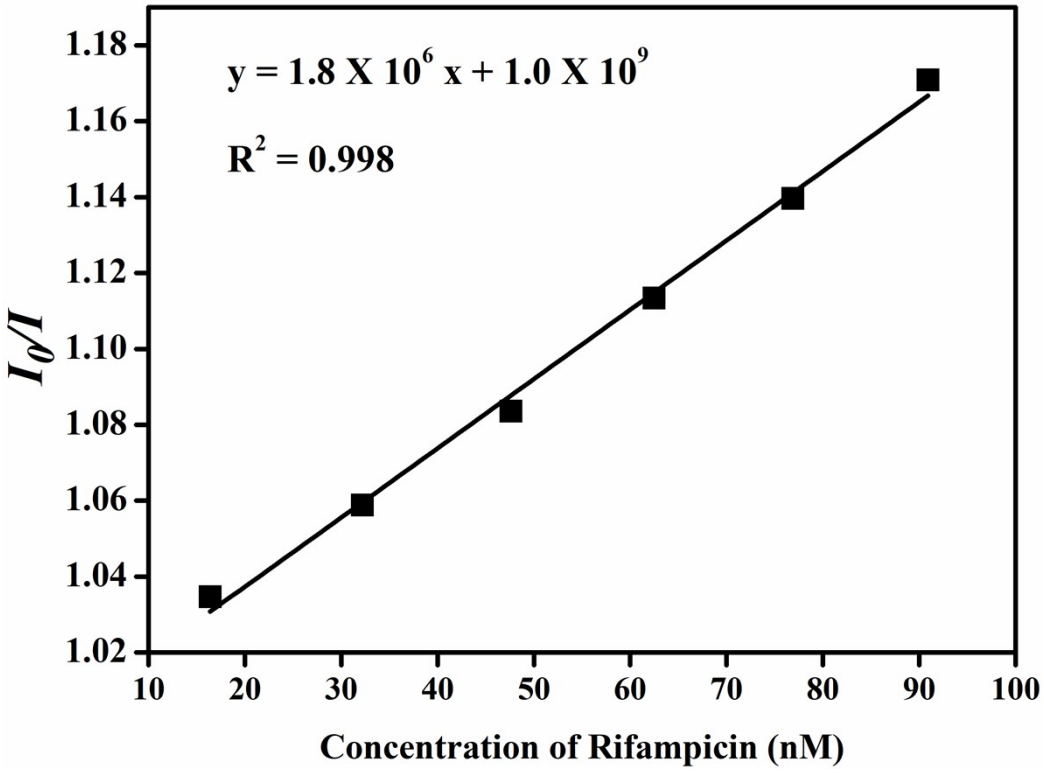

Figure S28. Stern-Volmer plot for **1′** with the incremental addition of rifampicin solution.

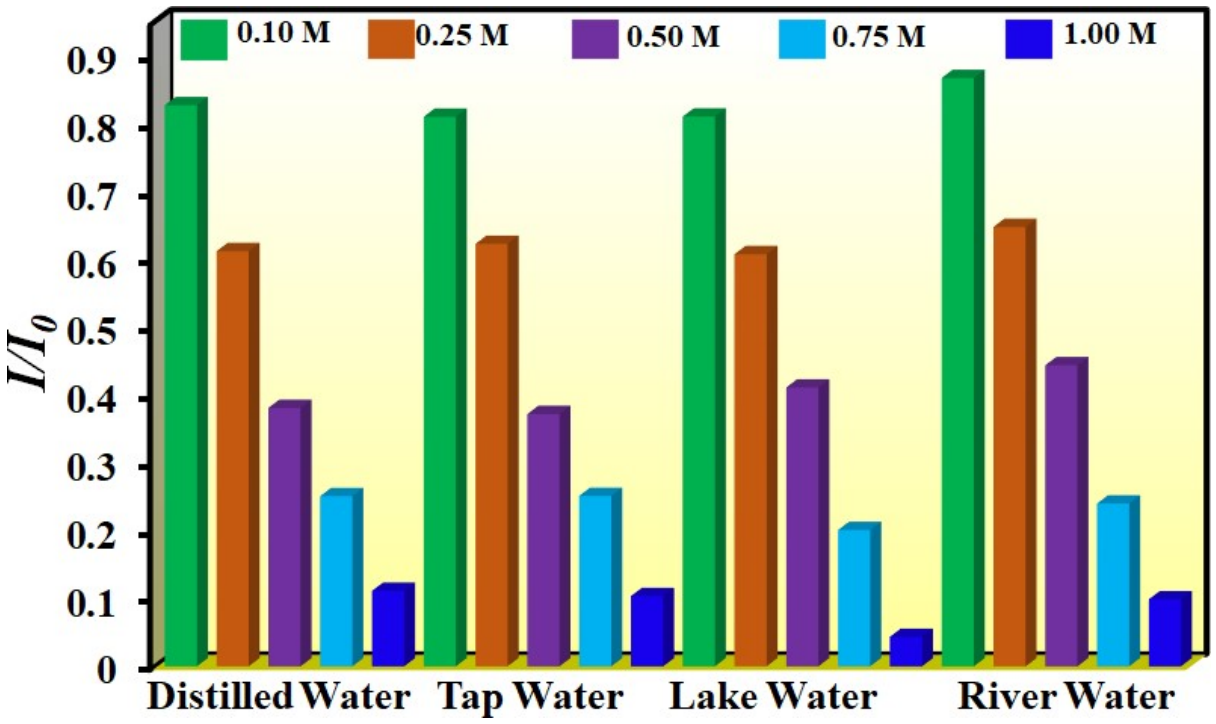

Figure S29. Bar plot depicting the detection of rifampicin from real water specimens by **1′**.

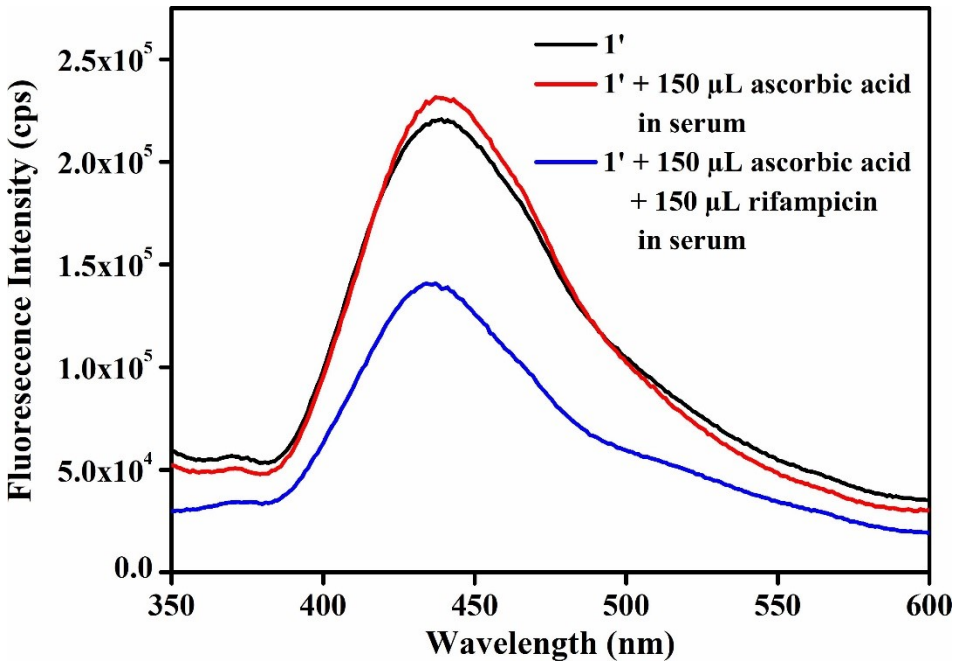

Figure S30. Fluorescence intensity of **1′** in human blood serum in presence of only ascorbic acid (red) and mixture of ascorbic acid and rifampicin (blue).

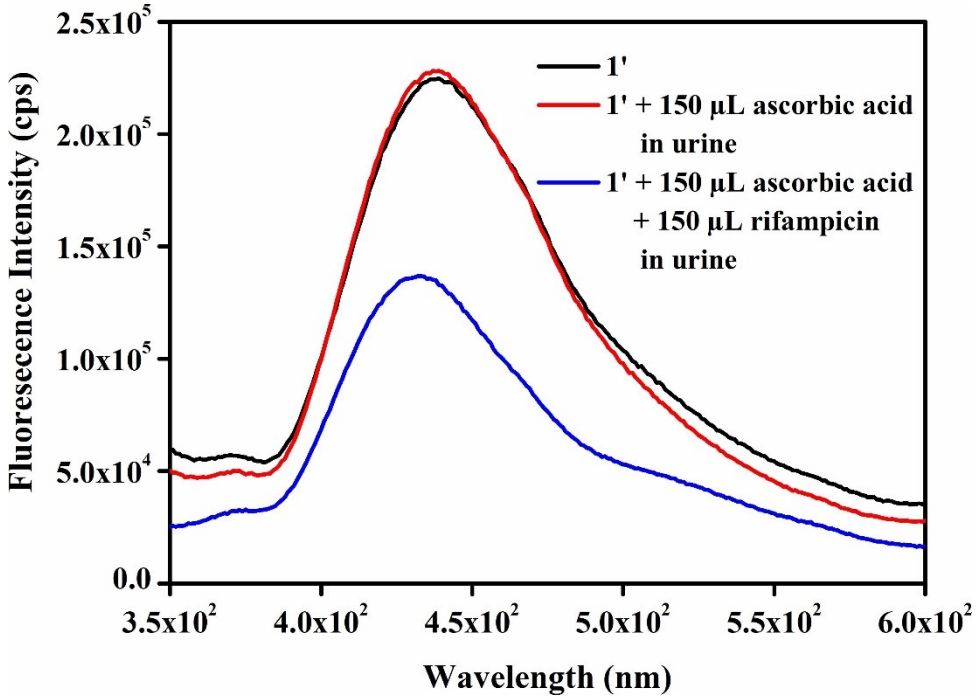

Figure S31. Fluorescence sensing of **1′** in human urine in presence of only ascorbic acid (red) and mixture of ascorbic acid and rifampicin (blue).

Table S2. Detection of rifampicin from human blood serum using **1′**.

Rifampicin Spiked (mol L^{-1})	Rifampicin Found (mol L^{-1})*	Recovery (%)	RSD (%) (n=3)
9.804×10^{-6}	9.541×10^{-6}	97.3	2.21
2.206×10^{-5}	2.322×10^{-5}	105.3	2.54
3.271×10^{-5}	3.222×10^{-5}	98.5	1.75

Table S3. Detection of rifampicin from human urine using **1′**.

Rifampicin Spiked (mol L^{-1})	Rifampicin Found (mol L^{-1})*	Recovery (%)	RSD (%) (n=3)
9.804×10^{-6}	9.311×10^{-6}	94.9	3.98
2.206×10^{-5}	2.361×10^{-5}	107.0	2.79
3.271×10^{-5}	3.073×10^{-5}	93.9	3.39

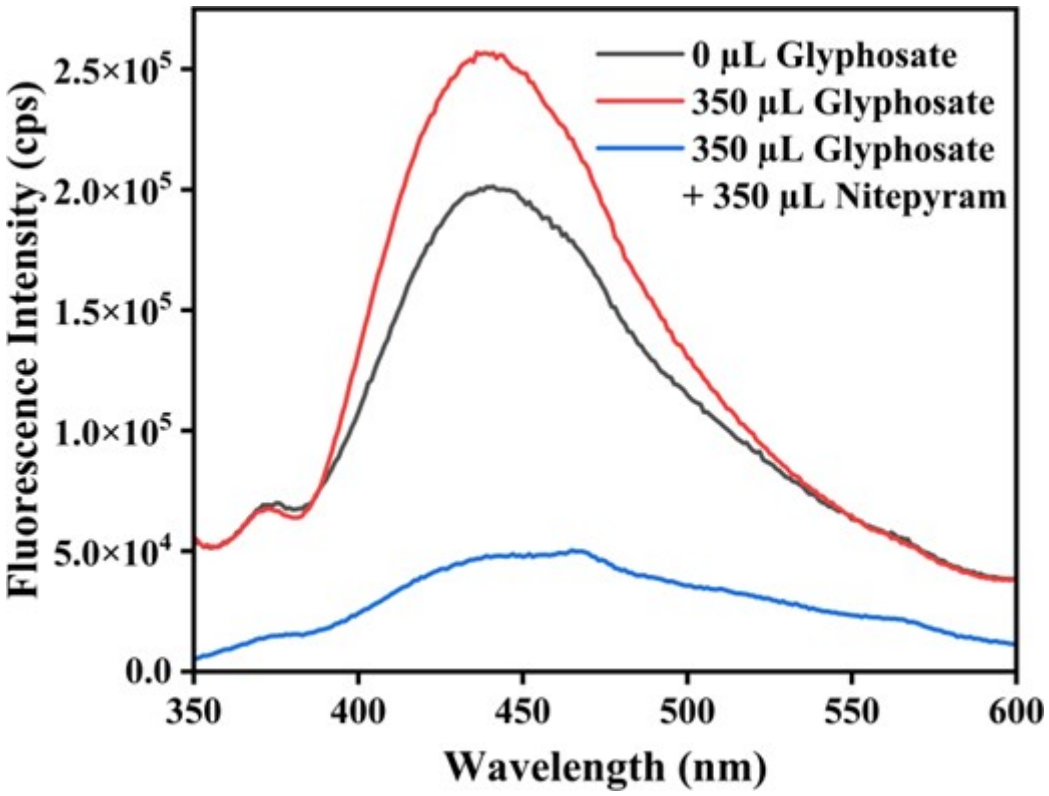

Figure S32. Fluorescence emission intensity of **1'** (black), **1'** in the presence of 300 µL of 5 mM aqueous glyphosate solution (red) and **1'** in the presence of both 300 µL of 5 mM aqueous glyphosate and rifampicin solution (blue).

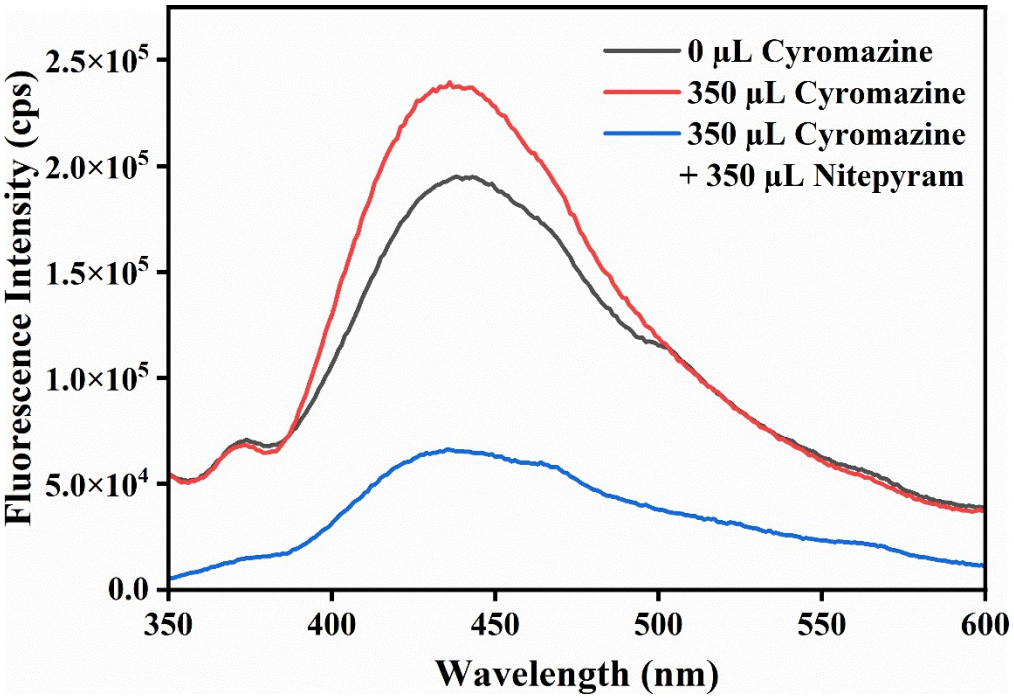

Figure S33. Fluorescence emission intensity of **1'** (black), **1'** in the presence of 300 µL of 5 mM aqueous cyromazine solution (red) and **1'** in the presence of both 300 µL of 5 mM aqueous cyromazine and rifampicin solution (blue).

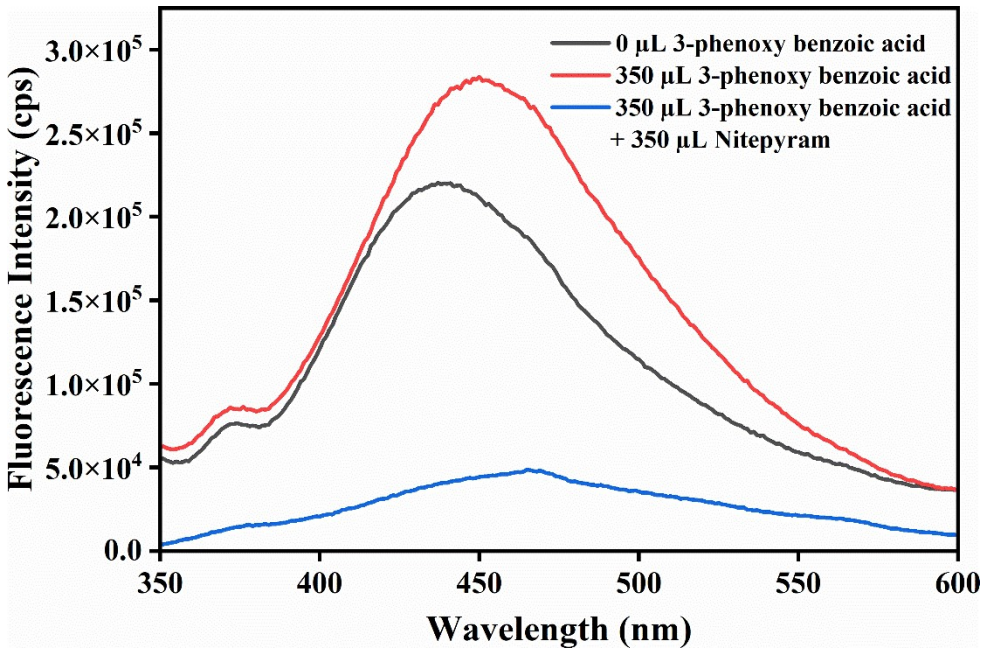

Figure S34. Fluorescence emission intensity of **1'** (black), **1'** in the presence of 300 µL of 5 mM aqueous 3-phenoxy benzoin acid solution (red) and **1'** in the presence of both 300 µL of 5 mM aqueous 3-phenoxy benzoin acid and rifampicin solution (blue).

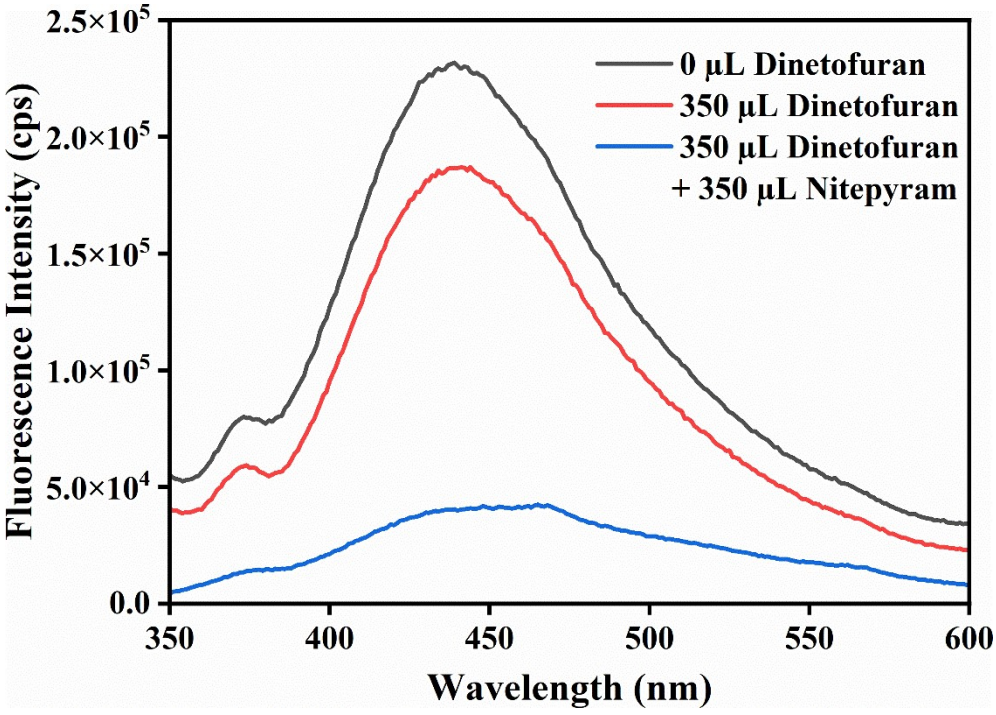

Figure S35. Fluorescence emission intensity of **1'** (black), **1'** in the presence of 300 µL of 5 mM aqueous dinetofuran solution (red) and **1'** in the presence of both 300 µL of 5 mM aqueous dinetofuran and rifampicin solution (blue).

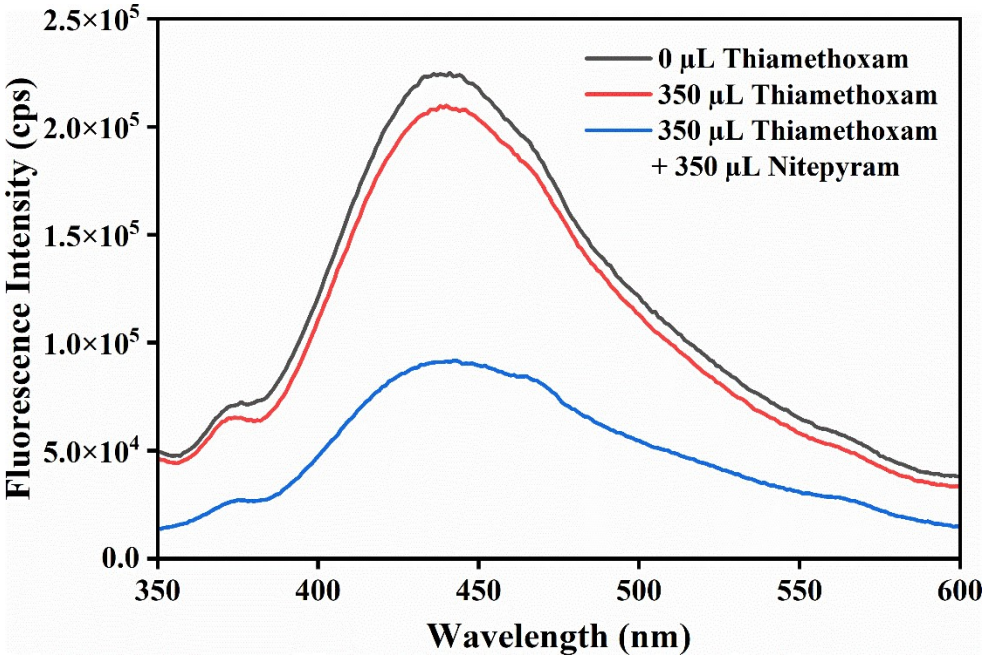

Figure S36. Fluorescence emission intensity of **1'** (black), **1'** in the presence of 300 µL of 1 mM aqueous thiamethoxam solution (red) and **1'** in the presence of both 300 µL of 1 mM aqueous thiamethoxam and rifampicin solution (blue).

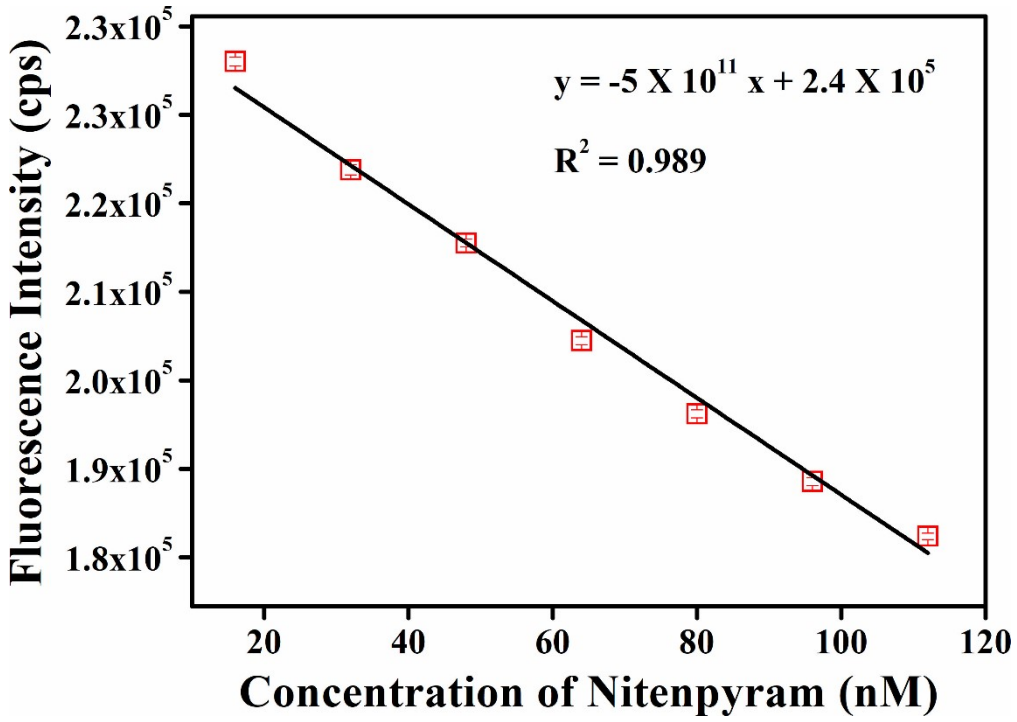

Figure S37. Plot of concentration of nitenpyram versus fluorescence intensity of **1'**.

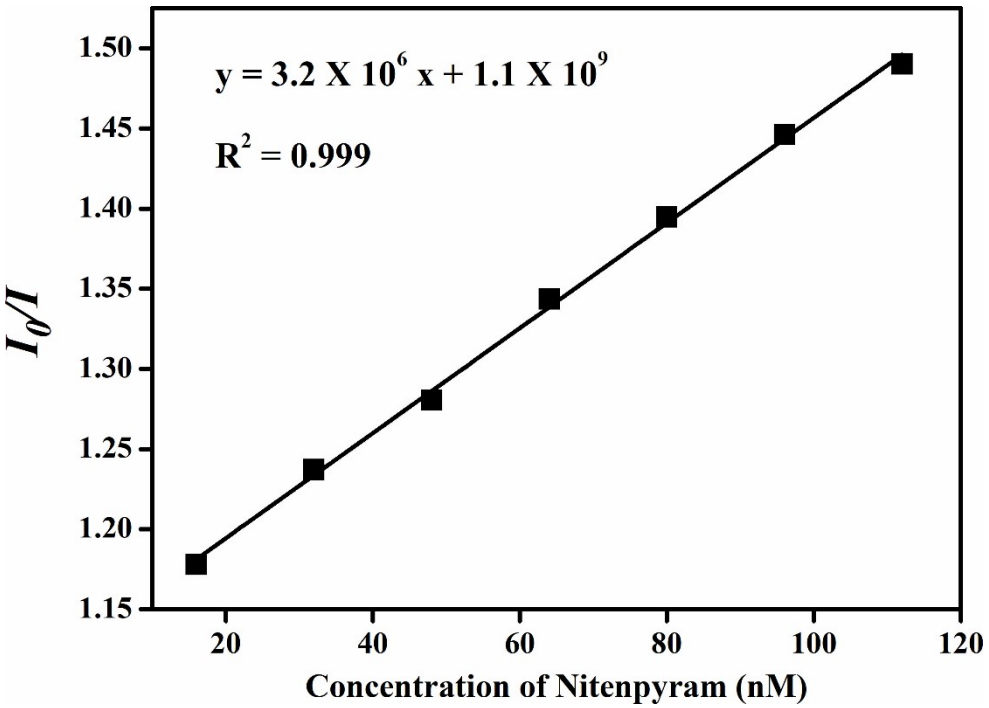

Figure S38. Stern-Volmer plot for **1′** with the incremental addition of nitenpyram solution.

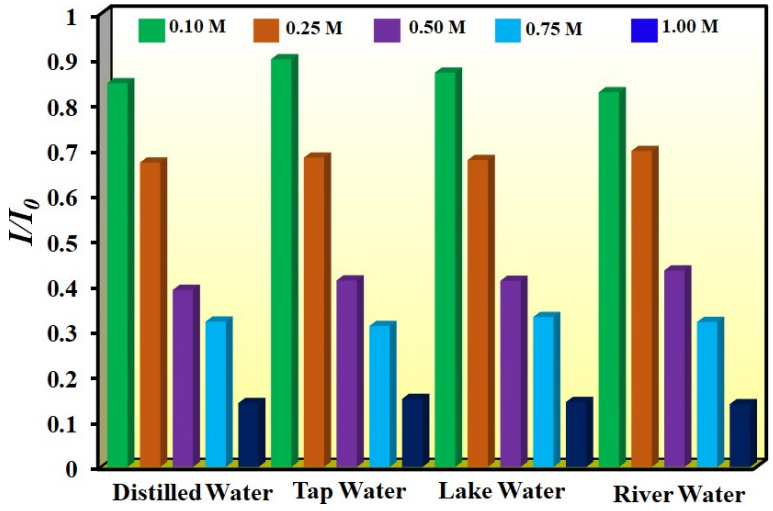

Figure S39. Bar plot depicting the detection of nitenpyram from real-water specimens by **1′**.

Table S4. Detection of nitenpyram from soil using **1′**.

Nitenpyram Spiked (mol L^{-1})	Nitenpyram Found (mol L^{-1})*	Recovery (%)	RSD (%) (n=3)
3.922×10^{-5}	3.891×10^{-5}	99.2	3.94
8.612×10^{-5}	8.873×10^{-5}	103.0	2.18
1.308×10^{-4}	1.278×10^{-4}	97.7	3.17

Table S5. Detection of nitenpyram from rice using **1′**.

Nitenpyram Spiked (mol L^{-1})	Nitenpyram Found (mol L^{-1})*	Recovery (%)	RSD (%) (n=3)
3.922×10^{-5}	4.103×10^{-5}	104.6	2.98
8.612×10^{-5}	8.838×10^{-5}	102.6	3.07
1.308×10^{-4}	1.295×10^{-4}	99.0	1.98

Table S6. Detection of nitenpyram from corn using **1′**.

Nitenpyram Spiked (mol L^{-1})	Nitenpyram Found (mol L^{-1})*	Recovery (%)	RSD (%) (n=3)
3.922×10^{-5}	4.137×10^{-5}	105.5	3.43
8.612×10^{-5}	8.986×10^{-5}	104.3	2.74
1.308×10^{-4}	1.292×10^{-4}	98.8	3.19

Table S7. Evaluation of intra-day, inter-day accuracy and precision parameters for change in fluorescence intensity of **1′** after incremental addition of 1 mM aqueous solution of rifampicin respectively.

Volume of Rifampicin Added	Intra-Day Fluorescence Emission Intensity (cps)			Mean (χ)	Standard Deviation (σ)	Relative Standard Deviation (RSD)
0 µL	254237	254252.2	253221.7	253903.6	482.2357	0.189
50 µL	175498.7	174478.8	174518.7	174832.1	471.6866	0.269
100 µL	118513.9	117911.6	117516.2	117980.6	410.2253	0.347
150 µL	94002.16	92999.91	93421.4	93474.4	410.8826	0.439
200 µL	58046.29	57995.36	59007.22	58349.6	465.4527	0.797
250 µL	34017.82	32945.46	33290.2	33417.8	446.9949	1.337
300 µL	19585.53	19193.82	19977.2	19585.5	319.8304	1.632
Volume of Rifampicin Added	Inter-Day Fluorescence Emission Intensity (cps)			Mean (χ)	Standard Deviation (σ)	Relative Standard Deviation (RSD)
0 µL	258754.5	258237	260565.8	258519.1	860.1	0.333
50 µL	176351.4	175998.7	177585.9	176478.7	554.6	0.314
100 µL	120955.8	120713.9	121802.5	120624.1	448.4	0.372
150 µL	94451.1	94262.2	95112.2	94641.81	409.8	0.433
200 µL	58062.4	57946.3	58468.8	58492.52	415.7	0.711
250 µL	33685.2	33617.8	33920.9	33674.66	385.3	1.144
300 µL	19624.8	19585.5	19762.2	19390.83	238.5	1.230

Table S8. Evaluation of intra-day, inter-day accuracy and precision parameters for change in fluorescence intensity of **1′** after incremental addition of 5 mM aqueous solution of nitenpyram.

Volume of Nitenpyram Added	Intra-Day Fluorescence Emission Intensity (cps)			Mean (χ)	Standard Deviation (σ)	Relative Standard Deviation (RSD)
0 µL	250900	251952	251548	251466.5	433.2	0.172
50 µL	186805	187120	187689	187204.9	365.8	0.195
100 µL	144381	143941	143317	143879.8	436.2	0.303
150 µL	104934	105012	105918	105287.8	446.6	0.424
200 µL	69925.6	69025.3	68896.6	69282.5	457.8	0.660
250 µL	43523.8	42912.1	42558.3	42998.1	398.8	0.927
300 µL	21536.6	20914.3	21817.5	21422.8	377.4	1.762
Volume of Nitenpyram Added	Inter-Day Fluorescence Emission Intensity (cps)			Mean (χ)	Standard Deviation (σ)	Relative Standard Deviation (RSD)
0 µL	250900	252859.5	251296.4	251685.3	845.9	0.336
50 µL	186805	187868.9	187501.5	187391.9	441.1133	0.235
100 µL	144381	144517.2	143174.1	144023.9	603.5273	0.419
150 µL	104734	105811.8	105432.1	105325.8	446.5384	0.423
200 µL	69925.6	69301.4	68727.7	69318.23	489.1841	0.705
250 µL	43523.8	42515.74	43183.75	43074.43	418.7348	0.972
300 µL	21536.6	21715.68	20907.96	21386.75	346.3592	1.619

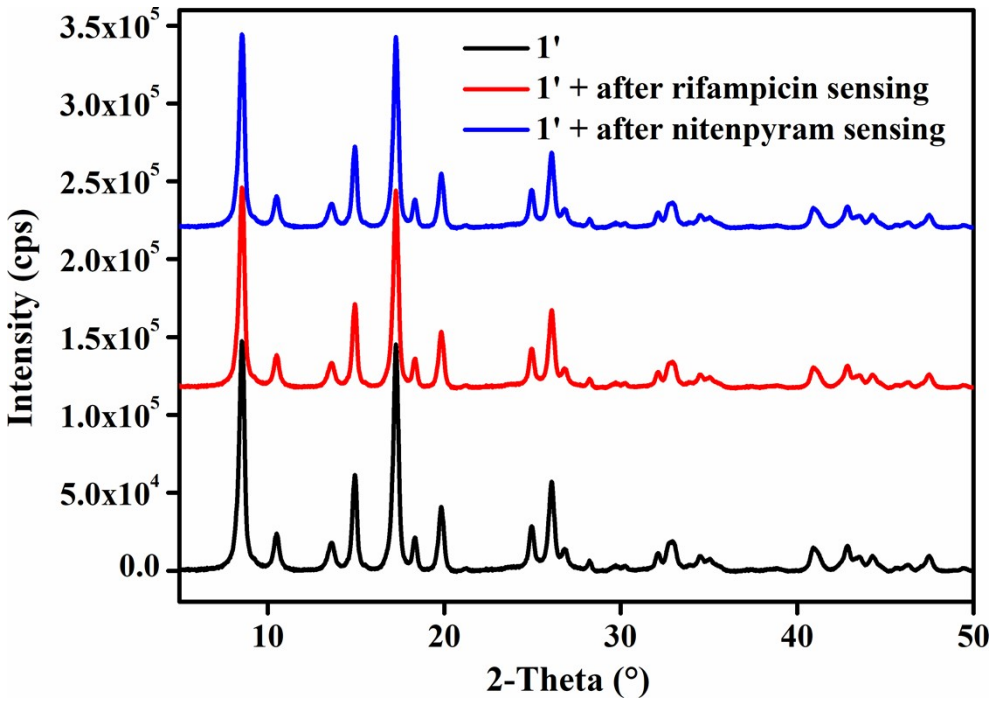

Figure S40. PXRD patterns of **1′** before sensing (black), after rifampicin sensing (red) and after nitenpyram sensing (blue).

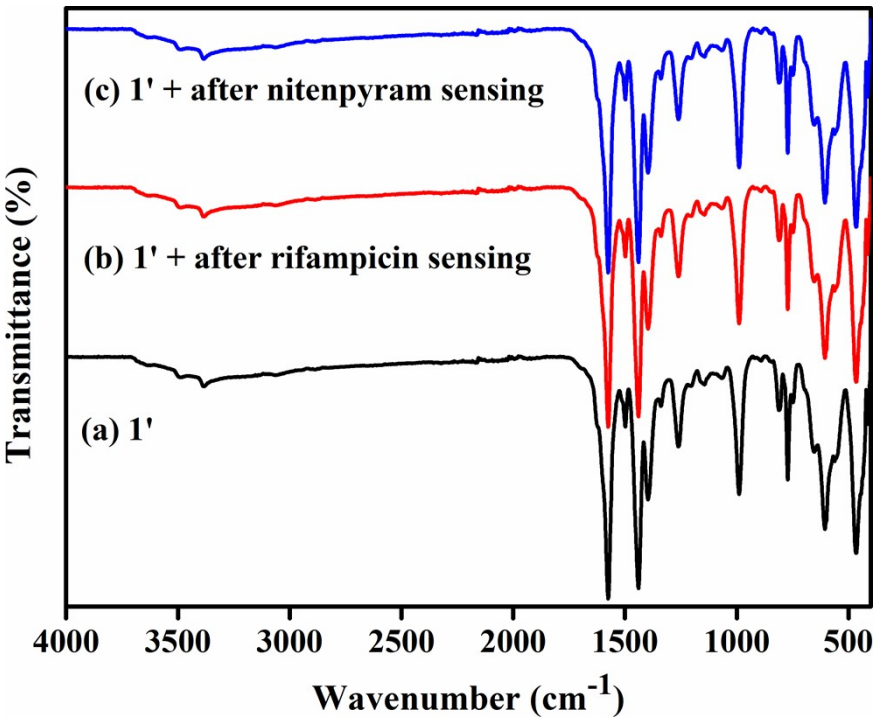

Figure S41. ATR-IR spectra of **1′** before sensing (black), after rifampicin sensing (red) and after nitenpyram sensing (blue).

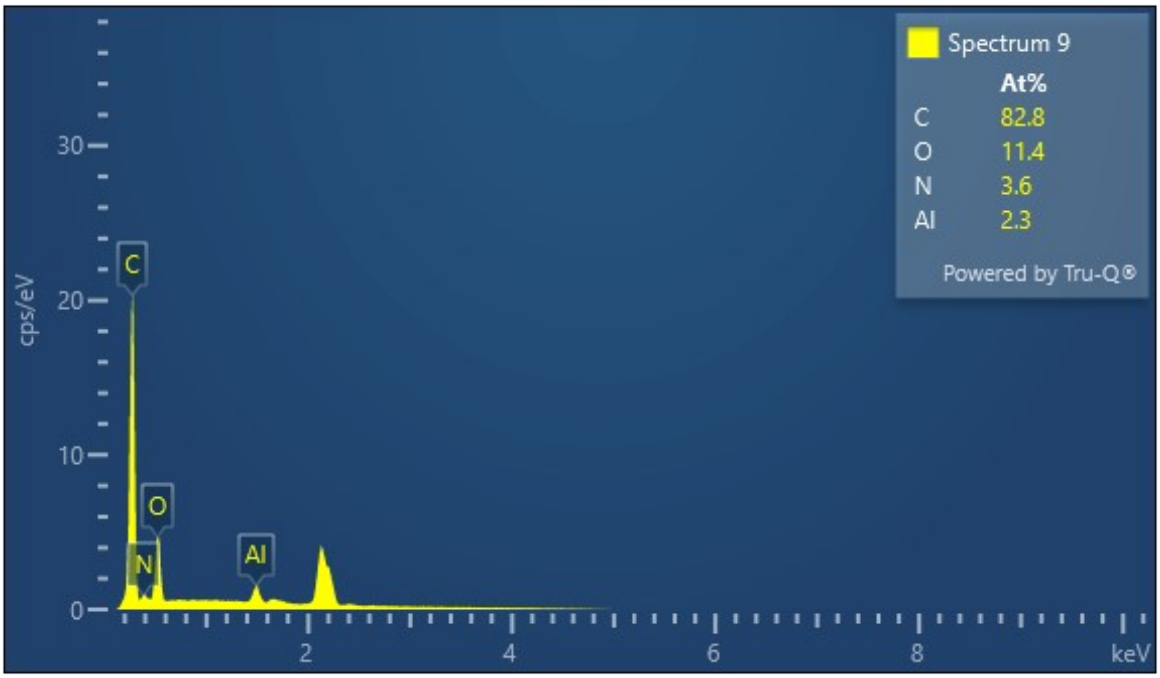

Figure S42. EDX elemental spectrum of **1′** after rifampicin sensing.

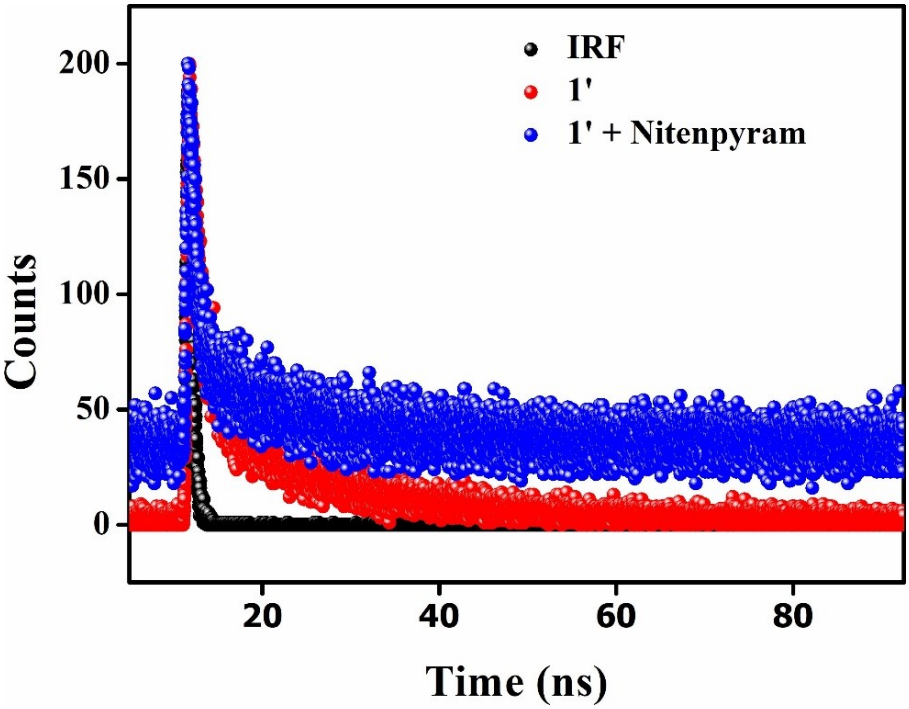

Figure S43. Time-resolved fluorescence lifetime decay plot for **1′** in presence and absence of rifampicin.

Table S9. Excited-state lifetime of **1′** in presence and absence of rifampicin.

Volume of Rifampicin Solution Added (μL)	B_1 (%)	B_2 (%)	T_1 (ns)	T_2 (ns)	$\langle\tau\rangle^*$ (ns)	χ^2
0	11.5	88.5	1.3	13.2	11.8	1.19
350	22.5	77.5	0.9	10.1	8.0	1.10

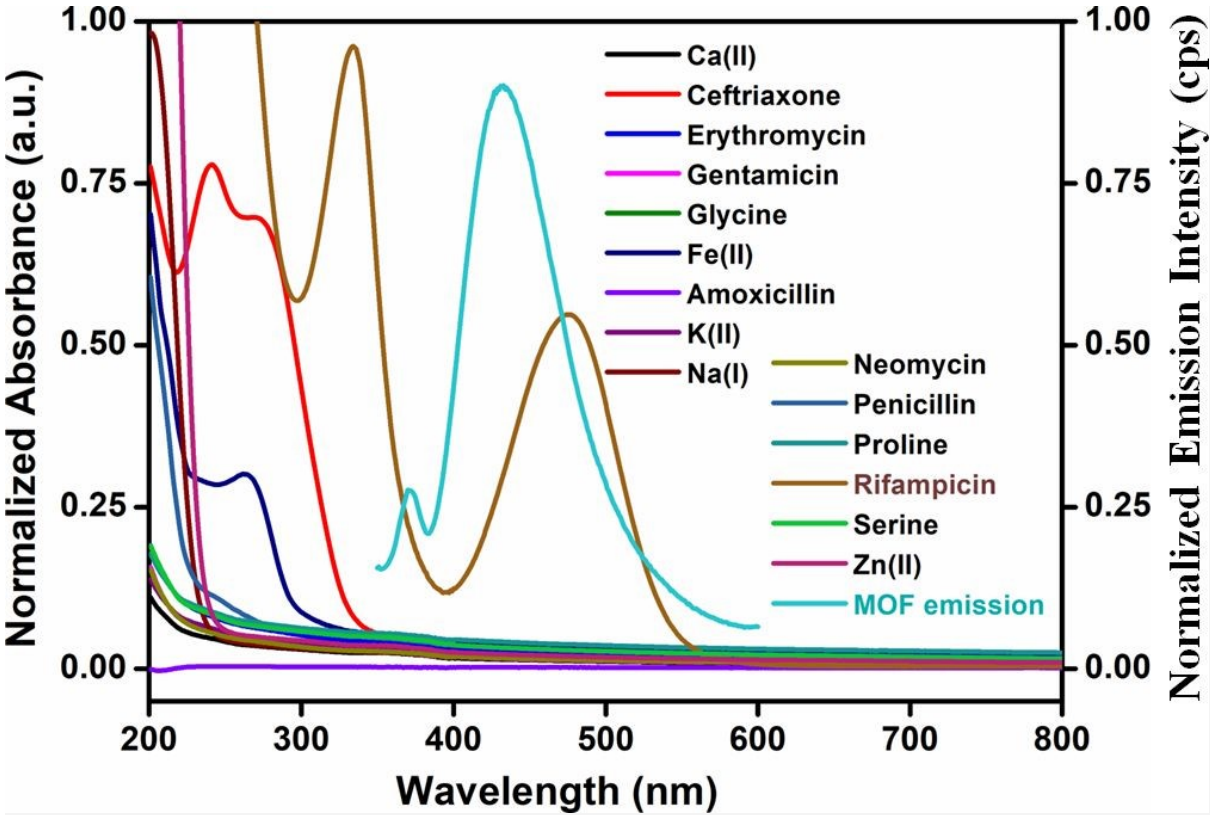

Figure S44. Overlap plot for UV-Vis spectra of all the analytes for rifampicin sensing with the fluorescence emission spectrum of **1′**.

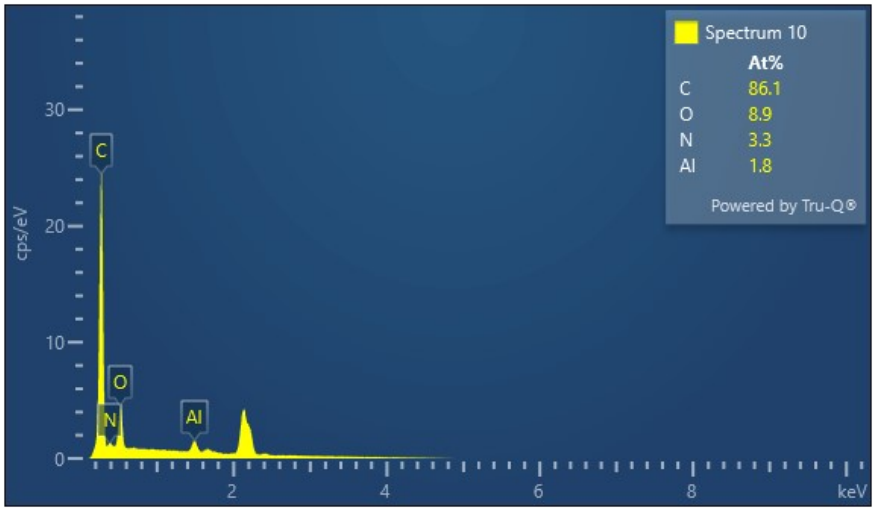

Figure S45. EDX elemental spectrum of **1′** after nitenpyram sensing.

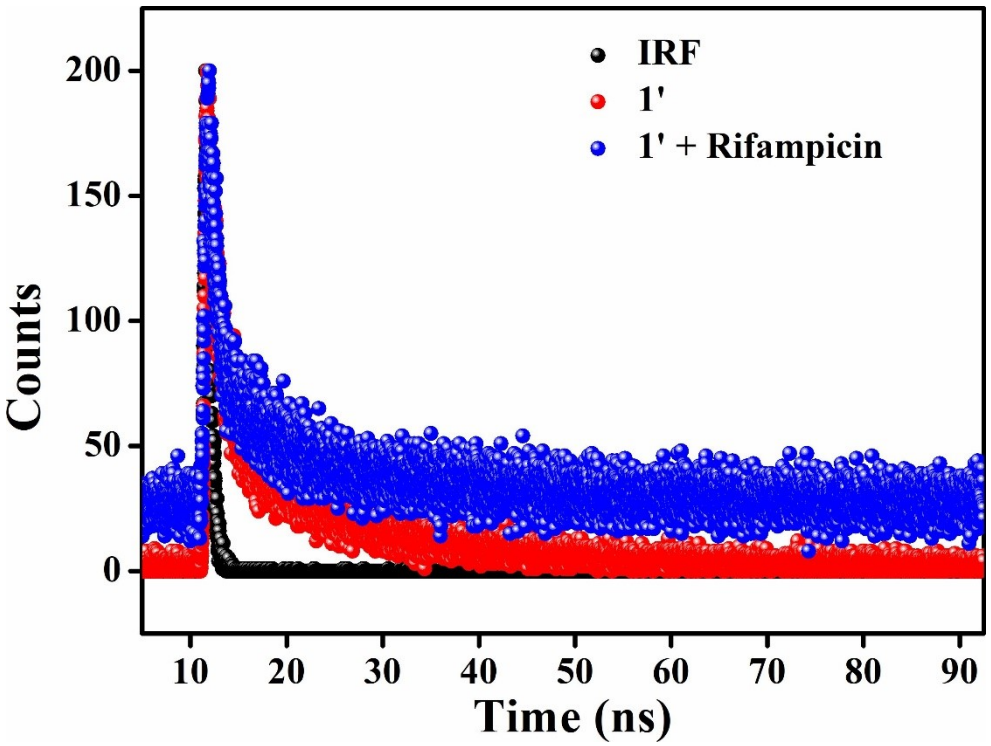

Figure S46. Time-resolved fluorescence lifetime decay plot for **1′** in presence and absence of nitenpyram.

Table S10. Excited-state lifetime of **1′** in presence and absence of nitenpyram.

Volume of Nitenpyram Solution Added (μL)	B_1 (%)	B_2(%)	T_1 (ns)	T_2 (ns)	$\langle\tau\rangle^*$ (ns)	χ^2
0	11.5	88.5	1.3	13.2	11.8	1.19
300	63.4	36.6	10.4	0.3	6.7	1.09

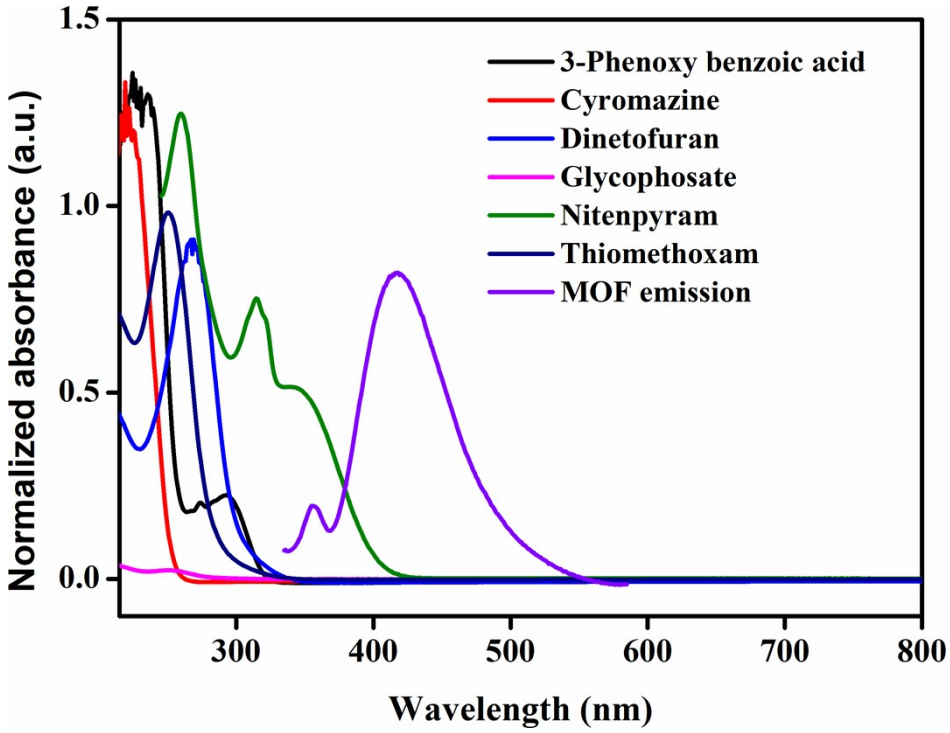

Figure S47. Overlap plot for UV-Vis spectra of analytes for nitenpyram sensing with the fluorescence emission spectrum of **1′**.

Table S11. Comparison table for fluorescence sensing performance of rifampicin by **1'** with previously reported materials.

Sl. No	Sensor Material	Material Type	Sensing Medium	LOD (nM)	Response Time (s)	K_{sv} (M^{-1})	Ref.
1	FA-Cu NCs	Nanocluster	methanol	0.07 µM	20 s	5.1×10^4	2
2	BSA-Au NCs	Nanocluster	water	0.09 µM	1800	-	3
3	G-NSCDs	Carbon dot	water	0.06 µM	1800	1.2×10^4	4
4	GSH-CdTe/ZnS QDs	Quantum dot	water	0.06 µM	900	4.4×10^4	5
5	Ce-N-CQDs	Cerium-Carbon Quantum dot	water	96 nM	300	-	6
6	**[Al(OH)(L)]·0.5 H_2O (1')**	**MOF**	**water**	**11.7 nM**	**5**	**1.8×10^6**	**this work**

Table S12. Comparison table for MOF based fluorescence sensing performance of nitenpyram with **1'**.

Sl. No	Sensor Material	Sensing Medium	LOD	Response Time (s)	K_{sv} (M^{-1})	Ref.
1	$[In_3Tb_3O_3(TATAB)_4(H_2O)_6]\cdot 12DMF\cdot 12H_2O$	water	0.63 μM	-	1.5×10^4	7
2	FMOF	water	0.11 μM	1200	-	8
3	Dye@MOFs	water	0.27 μM	-	-	9
4	EY@Zr-MOF	water	1.18 μM	-	3.5×10^4	10
5	**$[Al(OH)(L)]\cdot 0.5H_2O$ (1')**	**water**	**13.8 nM**	**5 s**	**3.2×10^6**	**this work**

References:

1. Das, A.; Anbu, N.; Sk, M.; Dhakshinamoorthy, A.; Biswas, S., Influence of hydrogen bond donating sites in UiO-66 metal-organic framework for highly regioselective methanolysis of epoxides. *ChemCatChem* **2020,** *12*, 1789-1798.
2. Zhang, Y.; Deng, Q.; Tang, C.; Zhang, M.; Huang, Z.; Cai, Z., Fluorescent folic acid-capped copper nanoclusters for the determination of rifampicin based on inner filter effect. *Spectrochim. Acta - A: Mol. Biomol. Spectrosc.* **2023,** *286*, 121944.
3. Chatterjee, K.; Kuo, C. W.; Chen, A.; Chen, P., Detection of residual rifampicin in urine via fluorescence quenching of gold nanoclusters on paper. *J. Nanobiotechnology* **2015,** *13*, 1-9.
4. Tang, X.; Zhao, Y.; Yu, H.; Cui, S.; Temple, H.; Amador, E.; Gao, Y.; Chen, M.-l.; Wang, S.; Hu, Z., Concentration-regulated multi-color fluorescent carbon dots for the detection of rifampicin, morin and Al3+. *Mater. Today Adv.* **2023,** *18*, 100383.
5. Hooshyar, Z.; Bardajee, G. R., Fluorescence enhancement of glutathione capped CdTe/ZnS quantum dots by embedding into cationic starch for sensitive detection of rifampicin. *Spectrochim. Acta - A: Mol. Biomol. Spectrosc.* **2017,** *173*, 144-150.
6. Sun, X.-H.; Ma, M.; Tian, R.; Chai, H.-M.; Wang, J.-W.; Gao, L.-J., One-pot hydrothermal method preparation of cerium–nitrogen-codoped carbon quantum dots from waste longan nucleus as a fluorescent sensor for sensing drug rifampicin. *ACS omega* **2023,** *8*, 34859-34867.
7. Li, A.; Chu, Q.; Zhou, H.; Yang, Z.; Liu, B.; Zhang, J., Effective nitenpyram detection in a dual-walled nitrogen-rich In (iii)/Tb (iii)–organic framework. *Inorg. Chem. Front.* **2021,** *8*, 2341-2348.

8. Liu, J.; Xiong, W. H.; Ye, L. Y.; Zhang, W. S.; Yang, H., Developing a novel nanoscale porphyrinic metal–organic framework: A bifunctional platform with sensitive fluorescent detection and elimination of nitenpyram in agricultural environment. *J. Agric. Food Chem.* **2020,** *68*, 5572-5578.
9. Yang, L.; Liu, Y.-L.; Liu, C.-G.; Ye, F.; Fu, Y., Two luminescent dye@ MOFs systems as dual-emitting platforms for efficient pesticides detection. *J. Hazard. Mater.* **2020,** *381*, 120966.
10. Wei, Z.; Chen, D.; Guo, Z.; Jia, P.; Xing, H., Eosin Y-embedded zirconium-based metal–organic framework as a dual-emitting built-in self-calibrating platform for pesticide detection. *Inorg. Chem.* **2020,** *59* (8), 5386-5393.